A *Francisella tularensis* L,D-carboxypeptidase plays important roles in cell morphology, envelope integrity, and virulence.

Briana Zellner[1], Dominique Mengin-Lecreulx[2], Brenden Tully[1], William T. Gunning 3rd[3], Robert Booth[3], Jason F. Huntley[1*]

[1] Department of Medical Microbiology and Immunology, University of Toledo, Toledo, OH, U.S.A.; [2] Université Paris-Saclay, CEA, CNRS, Institute for Integrative Biology of the Cell (I2BC), 91198, Gif-sur-Yvette, France; [3]Department of Pathology, University of Toledo, Toledo, OH, U.S.A.

Running Head: *F. tularensis* L,D-carboxypeptidase

To whom correspondence should be addressed: Jason F. Huntley, Department of Medical Microbiology and Immunology, University of Toledo College of Medicine and Life Sciences, 3000 Arlington Ave., MS1021, HEB 200D, Toledo, OH, U.S.A., 43614. Tel.: 419-383-5456; Email: Jason.Huntley@UToledo.edu

Summary

Francisella tularensis is a Gram-negative, intracellular bacterium that causes the zoonotic disease tularemia. Intracellular pathogens, including *F. tularensis*, have evolved mechanisms to survive in the harsh environment of macrophages and neutrophils, where they are exposed to cell envelope-damaging molecules. The bacterial cell wall, primarily composed of peptidoglycan (PG), maintains cell morphology, structure, and membrane integrity. Intracellular Gram-negative bacteria protect themselves from macrophage and neutrophil killing by recycling and repairing damaged PG – a process that involves over 50 different PG synthesis and recycling enzymes. Here, we identified a PG recycling enzyme, L,D-carboxypeptidase A (LdcA), of *F. tularensis* that is responsible for converting PG tetrapeptide stems to tripeptide stems. Unlike *E. coli* LdcA and most other orthologs, *F. tularensis* LdcA does not localize to the cytoplasm and also exhibits L,D-endopeptidase activity, converting PG pentapeptide stems to tripeptide stems. Loss of *F. tularensis* LdcA led to altered cell morphology and membrane integrity, as well as attenuation in a mouse pulmonary infection model and in primary and immortalized macrophages. Finally, an *F. tularensis ldcA* mutant protected mice against virulent Type A *F. tularensis* SchuS4 pulmonary challenge.

Keywords: tularemia, peptidoglycan, L,D-carboxypeptidase, virulence, *Francisella tularensis*

Introduction

The Gram-negative bacterial cell wall plays an important role in maintaining cell shape, protecting against external insults, and preventing cell lysis amid fluctuations in internal turgor pressure (Dhar, 2018). The cell wall is composed of peptidoglycan (PG), a network of alternating *N*-acetylglucosamine (GlcNAc) and *N*-acetylmuramic acid (MurNAc) glycan chains that are crosslinked through peptide stems, and lies just outside of the cytoplasmic membrane of most bacteria (Johnson, 2013, Mengin-Lecreulx & Lemaitre, 2005). In *Escherichia coli*, PG has been shown to be covalently attached to the outer membrane (OM) by Braun's lipoprotein and noncovalently attached by Pal and other lipoproteins (Braun, 1969, Braun, 1975, Bouveret, 1999, Leduc, 1992). A loss of membrane integrity can occur if interactions between PG and attached lipoproteins are disturbed, thus maintenance of correct PG architecture is extremely important (Braun & Rehn, 1969, Braun & Hantke, 2019).

Synthesis of Gram-negative PG precursors, studied mainly in *E. coli*, occurs in the bacterial cytoplasm and requires a series of enzymes to build a pentapeptide PG monomer before transporting this molecule into the periplasm. Periplasmic PG cross-linking most often occurs between the fourth residue (D-Ala) of newly-formed pentapeptide stems to the third residue (*meso*-A_2pm) of existing tripeptide stems (4-3 cross links), resulting in the release of the pentapeptide terminal D-Ala and forming tetrapeptide stems (Glauner, 1988, Pazos & Peters, 2019). PG is not a static structure, rather, PG degradation/remodeling is necessary to incorporate new PG and expand the cell wall during bacterial growth and replication, to insert flagella or secretion systems, and to septate during bacterial division (Scheurwater, 2008). Up to 60% of PG is recycled per generation, helping to repair damaged PG and providing energy during

periods of stress or starvation (Dhar, 2018, Park, 2008, Holtje, 1998). Using *E. coli* as a model, more than 50 different PG synthesis and hydrolysis/recycling enzymes have been identified, most of which appear to be cytoplasmic. While deletion studies in *E. coli* have indicated that some PG synthesis enzymes are essential, few PG hydrolases have been found to be essential and, in fact, substantial redundancy in hydrolase activity appears to exist. Indeed, alterations in cell morphology, membrane integrity, and ability to replicate/divide sometimes are observed only after multiple PG metabolism genes have been deleted (Dhar, 2018, van Heijenoort, 2011, Vollmer & Bertsche, 2008). Given the increasing threat of antimicrobial-resistant organisms and link between PG homeostasis and bacterial virulence, more studies are needed to understand how a diverse range of Gram-negative bacteria synthesize and recycle PG (Juan, 2018). Finally, PG studies can reveal new strategies to treat bacterial infections, as an *Acinetobacter baumannii* penicillin-binding protein (PBP) mutant was reported to be more sensitive to complement-mediated killing than wild-type bacteria (Russo, 2009) and a *Helicobacter pylori* PG hydrolase (AmiA) mutant was unable to colonize mouse stomachs (Chaput, 2016).

PG recycling, mainly characterized in *E. coli*, begins with periplasmic lytic transglycosylase (LT) cleavage of the β-1,4-glycosidic linkage between MurNAc and GlcNAc, forming a GlcNAc-1,6-anhydro-MurNAc product, which creates sites for the insertion of PG precursors and recycling of the GlcNAc-1,6-anhydro-MurNAc peptide (Scheurwater, 2008). Low molecular mass penicillin-binding proteins (LMM PBPs) can function as endopeptidases, cleaving the cross-links between adjacent tetrapeptide stems, and/or as D,D-carboxypeptidases, removing the terminal D-Ala of pentapeptides, forming the tetrapeptide (Dhar, 2018). Inner membrane permeases, such as AmpG, then transfer GlcNAc-1,6-anhydro-MurNAc disaccharides, with or without attached peptides, to the cytoplasm where they can be

disassembled. Cytoplasmic NagZ and AmpD further degrade disaccharides by cleaving the bond between GlcNAc and 1,6-anhydro-MurNAc, and separating the peptide chain from 1,6-anhydro-MurNAc, respectively. Additional cytoplasmic hydrolases, such as L,D-carboxypeptidases (Ldc), act on free peptide chains to cleave the terminal D-Ala from tetrapeptides, resulting in tripeptides (Dhar, 2018). PG is unusual in that it is both highly dynamic (*e.g.*, allowing for bacterial division and molecular transport across the periplasm), yet tightly regulated to prevent membrane collapse and bacterial death. As such, PG recycling enzymes have been speculated to be important virulence determinants in Gram-negative bacteria (Juan, 2018). Indeed, *E. coli ldc* mutants lyse in stationary phase (Templin, 1999) and are more susceptible to β-lactam antibiotics (Ursinus, 1992), *Helicobacter* and *Campylobacter ldc* mutants have altered cell morphology and defects in motility and biofilm formation (Sycuro, 2013, Frirdich, 2012, Frirdich, 2014), and *Neisseria gonorrhoeae ldc* mutants are unable to stimulate NOD1-dependent responses in the host (Lenz, 2017). However, very little is known about the importance of PG recycling enzymes in the pathogenesis of intracellular pathogens such as *Francisella tularensis*.

F. tularensis, the causative agent of tularemia, is a Gram-negative, intracellular, coccobacillus that can infect and cause lethal disease in many species, including humans (Dennis, 2001, Keim, 2007). There are three subspecies of *F. tularensis*, subsp. *tularensis* (Type A), subsp. *holarctica* (Type B), and subsp. *mediasiatica*, although only subsp. *tularensis* and subsp. *holarctica* are virulent for humans (Kingry, 2014). *F. tularensis* poses a severe threat to public health and has been classified as an NIH Category A Priority Pathogen and a CDC Tier 1 Select Agent due to its low infectious dose (<10 CFU), ease of aerosolization, and high morbidity and mortality rates (up to 60%) (Ellis, 2002, Sjostedt, 2007). Like other intracellular pathogens, *F. tularensis* has evolved different mechanisms to infect, survive, and replicate within

host cells, including macrophages and neutrophils (Ray, 2009). However, this lifestyle exposes the bacteria to reactive oxygen species (ROS), reactive nitrogen species (RNS), antimicrobial peptides, and other cell membrane- and cell wall-damaging molecules (Jones, 2012). Our group previously demonstrated that the *F. tularensis* disulfide bond formation protein A (DsbA) ortholog repairs damaged outer membrane proteins and known virulence factors. We additionally showed that *F. tularensis* DsbA, unlike periplasmic DsbA in *E. coli* and most other Gram-negative bacteria, is outer membrane-bound and is a multifunctional protein with both oxidoreductase and isomerase activities. Finally, using a molecular trapping approach, we identified over 50 *F. tularensis* DsbA substrates, many of which we speculate are involved in virulence (Ren, 2014).

Here, we determined the function of one of those *F. tularensis* DsbA substrates – a previously unstudied hypothetical protein containing a putative LdcA domain – and assessed its role in bacterial virulence. Deletion of *F. tularensis ldcA* resulted in bacteria with altered cell morphology, increased sensitivity to β-lactam antibiotics, yet increased resistance to several stressors (*e.g.*, H_2O_2, NaCl, low pH). Next, we demonstrated that *F. tularensis* LdcA exhibits L,D-carboxypeptidase and L,D-endopeptidase activities on pentapeptide and tetrapeptide residues of PG. Finally, we established that *F. tularensis* LdcA is required for virulence, as mutants were unable to replicate in macrophages or cause disease in mice.

Results

FTL1678 contains a putative L,D-carboxypeptidase domain

Previous studies by our group and others have shown that *F. tularensis* DsbA mutants are attenuated in mice (Qin, 2009, Ren, 2014). However, additional work by our group,

demonstrating that DsbA possesses both oxidoreductase and isomerase activities to repair damaged envelope and cell membrane proteins, indicated that other envelope proteins likely are responsible for *F. tularensis* virulence (Ren, 2014). To identify new *F. tularensis* virulence factors, we used a molecular trapping approach and identified over 50 *F. tularensis* DsbA substrates (Ren, 2014). One of those DsbA substrates, FTL1678, is annotated in the *F. tularensis* genome as a conserved membrane hypothetical protein. Here, a conserved domain search revealed that a large portion of FTL1678 contains a putative Ldc domain, part of the peptidase_S66 superfamily (Figure S1). Ldc proteins have been studied in a number of Gram-negative bacteria, including *E. coli* (Metz, 1986a, Templin, 1999, Metz, 1986b, Ursinus, 1992), *Pseudomonas aeruginosa* (Korza, 2005), *N. gonorrhoeae* (Lenz, 2017), and *Campylobacter jejuni* (Frirdich, 2014). To further explore this conserved domain, amino acid sequences of FTL1678 (*F. tularensis* subsp. *holarctica* [Type B] LVS) and FTT0101 (homolog of FTL1678 in *F. tularensis* subsp. *tularensis* [Type A] SchuS4) were aligned with LdcA orthologs from *E. coli*, *P. aeruginosa*, *N. gonorrhoeae*, and *C. jejuni* (named Pgp2). Despite low percentages of amino acid identities among the LdcA orthologs (6.3% to 30.3%; Figure 1), there was a higher degree of amino acid similarity among LdcA orthologs (13.0% [*E. coli* and *C. jejuni*] to 44.7% [*E. coli* and *N. gonorrhoeae*]; Figure 1). Notably, the LdcA Ser-Glu-His catalytic triad, previously shown to be required for *P. aeruginosa* LdcA activity (Korza, 2005), was absent from *C. jejuni* Pgp2 but was present in all LdcA homologs, including FTL1678 and FTT0101 (Figure 1).

FTL1678 exhibits L,D-carboxypeptidase and L,D-endopeptidase activities

To confirm the predicted Ldc activity of FTL1678 and FTT0101, recombinant FTL1678 and FTT0101 were expressed and affinity purified from *E. coli*. As a control, lysates from *E. coli*

containing the empty expression vector (pPROEX HTb) also were affinity-purified. PG precursors and PG intermediates were prepared as previously described (Herve, 2007, Blanot, 1983, Pennartz, 2009, Leulier, 2003, Stenbak, 2004). HPLC retention times for all PG substrates and products are listed in Table S1. Recombinant FTL1678, lysate from the vector control, or buffer alone were incubated with various PG substrates (Table 1) to determine substrate specificity and specific activity. The vector control and buffer alone did not demonstrate activity against any of the PG substrates (Figure S2 and S3). When FTL1678 was incubated with various PG substrates, the highest specific activity was detected against the tetrapeptide substrates GlcNAc-anhydroMurNAc-L-Ala-γ-D-Glu-*meso*-A_2pm-D-Ala (tracheal cytotoxin; TCT; 21.5 nmol/min/mg of protein; Table 1) and GlcNAc-MurNAc-L-Ala-γ-D-Glu-*meso*-A_2pm-D-Ala (reducing PG monomer; 15.6 nmol/min/mg of protein; Table 1), confirming that FTL1678 exhibits L,D-carboxypeptidase activity. Interestingly, FTL1678 activity against free tetrapeptide, L-Ala-γ-D-Glu-*meso*-A_2pm-D-Ala, was approx. 6-fold lower (3.4 nmol/min/mg of protein; Table 1) than TCT and 5-fold lower than the reducing PG monomer (Table 1), indicating that GlcNAc and MurNAc may be important for tetrapeptide recognition or FTL1678 binding. Next, FTL1678 was found to exhibit negligible activity against L-lysine-containing substrates (0.7 to 1.3 nmol/min/mg of protein; Table 1), where L-lysine replaced *meso*-A_2pm at the third amino acid position, indicating the importance of *meso*-A_2pm. Importantly, FTL1678 exhibited specific activity against pentapeptide substrates MurNAc-L-Ala-γ-D-Glu-*meso*-A_2pm-D-Ala-D-Ala (9.8 nmol/min/mg of protein; Table 1) and UDP-MurNAc-L-Ala-γ-D-Glu-*meso*-A_2pm-D-Ala-D-Ala (5.9 nmol/min/mg of protein; Table 1), indicating that FTL1678 also functions as an L,D-endopeptidase (cleavage of the pentapeptide between *meso*-A_2pm and D-Ala). D-Ala-D-Ala, but not D-Ala, was released in that case, confirming that FTL1678 did not display D,D-

carboxypeptidase activity. FTL1678 was not inhibited by 5 mM EDTA and did not require the presence of cations (Mg^{2+}) for tetrapeptide cleavage (Figure S3).

To further investigate the endopeptidase activity of FTL1678, FTL1678 was incubated with various TCT monomer and dimer substrates, containing different peptide lengths and cross-link locations (Table S2). Although FTL1678 exhibited the highest specific activity against TCT monomers containing tetrapeptide stems with either an alanine or a glycine in the fourth position (20.1 nmol/min/mg and 18.0 nmol/min/mg of protein, respectively; Table S2), FTL1678 also was able to cleave all four variations of the TCT dimer (two cross-linked TCT monomers; Table S2). Together, these results demonstrated that FTL1678 exhibited both L,D-carboxypeptidase and L,D-endopeptidase activities. Of the four different TCT dimer analogs tested, FTL1678 was most active on TCT dimers connected by a 4-3 (D-D) D-Ala-*meso*-A_2pm cross linkage (6.6 nmol/min/mg of protein; Table S2), followed by an approx. 24-fold reduction in activity on 3-3 (L-D) A_2pm-A_2pm cross links connecting two tripeptides (0.28 nmol/min/mg of protein; Table S2), a tripeptide and tetrapeptide with a glycine at the fourth position (0.21 nmol/min/mg of protein; Table S2), and a tripeptide and tetrapeptide with an alanine at the fourth position (0.16 nmol/min/mg of protein; Table S2). These data suggest that, while FTL1678 exhibits endopeptidase activity on 4-3 and 3-3 cross-linked dimers, cleavage of 3-3 cross links is likely not its main physiological function.

Assays were repeated with recombinant FTT0101 (SchuS4 homolog) and, due to 99.4% amino acid identify with FTL1678, FTT0101 demonstrated similar tetrapeptide cleavage activity (*i.e.*, LdcA activity) as FTL1678 (Table 1). FTT0101 also was not active on a peptidoglycan polymer and had either no or negligible activity on PG monomers that were amidated at the *meso*-A_2pm or D-Glu residues (Table 1).

As highlighted in Figure 1, a Ser-Glu-His catalytic triad was found in five of six Ldc orthologs examined here, including FTL1678 and FTT0101. However, *C. jejuni* Pgp2, which has been shown to exhibit LdcA activity (Frirdich, 2014), lacks the Ser-Glu-His catalytic triad, indicating that a Ser-Glu-His catalytic triad may not be required for LdcA function. As such, we speculated that single amino acid mutations of the putative Ser134-Glu239-His308 catalytic triad in FTL1678 may not be sufficient to abolish enzyme function. Recombinant FTL1678 mutant proteins were generated and purified, each containing either two amino acid mutations (S134A/E239A, S134A/H308A, and E239A/H308A) or three amino acid mutations (S134A/E239A/H308A). Similar to what is described above, enzymatic assays were performed, using the TCT monomer as a substrate. While no specific activity to TCT monomer was detected for the empty vector control or buffer alone (Figure S2), WT FTL1678 was active against the TCT monomer (21.5 nmol/min/mg; Table S3). By comparison, no activity was detected for any of the double or triple mutant proteins (Table S3), indicating that mutation of two of more amino acids of the putative Ser134-Glu239-His308 catalytic triad ablates FTL1678 Ldc activity. Analysis of single amino acids of the putative Ser134-Glu239-His308 catalytic triad are described below.

FTL1678 is OM-associated

E. coli and *P. aeruginosa* Ldcs have been localized to the bacterial cytoplasm (Templin, 1999, Korza, 2005). However, *C. jejuni* Pgp2 is unusual in that it contains a signal peptide and has been speculated to be periplasmic (Frirdich, 2014). In addition, *N. gonorrhoeae* LdcA was found to be periplasmic and outer membrane-associated (Lenz, 2017). As noted above, we previously demonstrated that FTL1678 is a DsbA substrate (Ren, 2014), indicating that FTL1678

is located in the *F. tularensis* envelope (*i.e.*, in the inner membrane [IM], periplasm, or outer membrane [OM]). Bioinformatic analyses of FTL1678 indicated that it is a periplasmic protein due to the presence of a signal peptide but absence of OM or lipoprotein signatures (Table S4). To experimentally confirm FTL1678 localization, we generated an *F. tularensis* strain with 6× histidine-tagged FTL1678, then performed spheroplasting, osmotic lysis, and sucrose density gradient centrifugation to separate IM and OM fractions and probe for protein subcellular localization. Immunoblotting of whole-cell lysates (WCL), OM fractions, and IM fractions demonstrated that the OM control protein, FopA (Huntley, 2007), only was present in WCL and OM fractions (but not IM fractions; Figure 2) and the IM control protein, SecY (Huntley, 2007), only was present in WCL and IM fractions (but not OM fractions; Figure 2). By comparison, FTL1678 only was detected in WCL and OM fractions, demonstrating OM-association (Figure 2). As noted above, because *N. gonorrhoeae* LdcA was found to fractionate to both the OM and soluble fractions (indicating periplasmic localization) (Lenz, 2017), we next examined the localization of *F. tularensis* periplasmic proteins in our fractions to better understand FTL1678 localization. TolB is a well-known periplasmic protein in Gram-negative bacteria and binds to PG due to its interaction with the peptidoglycan associated lipoprotein, Pal (Clavel, 1998, Walburger, 2002). We previously demonstrated that the *F. tularensis* Pal homolog is OM-localized (Huntley, 2007), similar to its OM-localization in other Gram-negative bacteria. Here, the *F. tularensis* TolB homolog was detected in OM fractions, but not IM fractions (Figure S4), indicating that *F. tularensis* PG-associated proteins also fractionate with OMs. In summary, data that FTL1678 is a DsbA substrate (*i.e.*, FTL1678 is an envelope protein)(Ren, 2014), FTL1678 contains a signal peptidase I cleavage site (Table S4), FTL1678 does not contain membrane protein signatures (Table S4), and FTL1678 is OM-associated (Figure 2), provides strong

253 evidence that FTL1678 is not a cytoplasmic protein, unlike *E. coli* LdcA. Instead, our data
254 indicate that, similar to *N. gonorrhoeae* LdcA, FTL1678 may be a periplasmic protein.
255
256 *Deletion of FTL1678 alters bacterial morphology*
257 LdcA has been shown to be important for maintenance of bacterial morphology and
258 structural integrity (Sycuro, 2013, Frirdich, 2014). In addition, mutations/deletions or
259 combinations of mutations/deletions in PG-modifying proteins can result in abnormal bacterial
260 morphology, emphasizing the importance of PG modification and recycling (Nelson, 2000,
261 Guinane, 2006, Priyadarshini, 2007, Heidrich, 2001, Sycuro, 2010, Juan, 2018). To assess if
262 FTL1678 plays a similar role in *F. tularensis*, we generated an isogenic deletion of *FTL1678*,
263 referred to hereafter as Δ*FTL1678*, in *F. tularensis* LVS. When examined by transmission
264 electron microscopy (TEM), wild-type (WT) bacterial width ranged from 350 to 800 nm (Figures
265 3A and 3D), whereas Δ*FTL1678* bacteria were more uniform in cell width, averaging approx.
266 350 nm (Figures 3B and 3D). While WT bacteria generally were observed to be coccobacilli
267 (Figure 3A), Δ*FTL1678* bacteria were found to be more coccoid in appearance, the Δ*FTL1678*
268 OM was more tightly-associated than WT OMs, and three electron dense structures, likely the
269 OM, PG, and IM, were present around the periphery of the majority of Δ*FTL1678* bacterium
270 (Figure 3B), compared to less prominent outer structures surrounding WT bacteria (Figure 3A).
271 Additionally, Δ*FTL1678* bacteria appeared more electron dense and had significantly-thicker
272 OMs than WT bacteria (Figures 3A, 3B, and 3C).
273 Previous studies have shown that deletion of genes for PG-modifying proteins (*e.g.*,
274 murein hydrolases) can result in abnormal growth characteristics, including lysis during
275 stationary phase (Templin, 1999) and an inability to separate daughter cells at the septa during

cell division, resulting in abnormal bacterial chains (Heidrich, 2002, Denome, 1999, Priyadarshini, 2006, Priyadarshini, 2007, Heidrich, 2001, Chaput, 2016, Juan, 2018, Weaver *et al.*, 2019). Although *N*-acetylmuramyl-L-alanine amidases have been shown to be predominantly involved in the cleavage of bacterial septa, deletion of lytic transglycosylases and some endopeptidases, in combination with amidase deletions, also have resulted in abnormal bacterial chains (Heidrich, 2001, Heidrich, 2002). To examine any potential replication defects of Δ*FTL1678*, we compared both OD_{600} values (Figure S5A) and CFUs over time (Figure S5B) of WT and Δ*FTL1678* in supplemented Mueller-Hinton Broth (sMHB; standard growth medium for *F. tularensis*; (Huntley, 2007)), finding that Δ*FTL1678* did not have any inherent growth defects. When examining both WT and Δ*FTL1678* by TEM for any septation defects or abnormal bacterial chains, approximately 10% of Δ*FTL1678* bacteria grew in chains of three to four bacteria (Figure S6A and S6B), whereas no WT bacteria exhibited this septation defect (data not shown). Taken together, our findings that Δ*FTL1678* is 1.5- to 2-times smaller than WT (Figure 3D), Δ*FTL1678* is more coccoid in shape (Figure 3B), Δ*FTL1678* has a thicker OM (Figure 3B and 3C), and Δ*FTL1678* has a partial septum defect (Figure S6), further support the role of FTL1678 as a PG-modifying enzyme that is important for bacterial elongation and division.

To provide additional evidence that alterations in Δ*FTL1678* morphology were solely due to loss of FTL1678 Ldc activity, we sought to complement Δ*FTL1678* with either *FTL1678* or a known LdcA and assess restoration of WT bacterial morphology. Although *E. coli* and *P. aeruginosa* LdcA orthologs contain the Ser-Glu-His catalytic triad (Figure 1), those LdcA orthologs are cytoplasmic and, given our data that FTL1678 is OM-localized and PG-associated (*i.e.*, may be periplasmic; Figure 2), we speculated that cytoplasmic LdcA orthologs may not

function in the *F. tularensis* periplasm. In contrast, *C. jejuni* Pgp2 has been shown to exhibit LdcA activity, has been speculated to be periplasmic (Frirdich, 2014), but lacks the Ser-Glu-His catalytic triad (Figure 1). To examine if *FTL1678* or *pgp2* could complement Δ*FTL1678*, we independently generated an *FTL1678 in trans*-complement and a *pgp2 in trans*-complement, examined bacterial morphologies of both complemented strains by TEM, and found that both complemented strains had similar morphologies as WT LVS (Figure S7A-B and Figure 3A). Additionally, OM thickness and cell width were measured for WT, Δ*FTL1678*, and both complemented strains, demonstrating that both complemented strains had OM thicknesses and cell widths similar to WT, and both complemented strains were significantly different from Δ*FTL1678* (Figure S7C-D). Taken together, these complementation studies provide further evidence that FTL1678 is an LdcA and that Δ*FTL1678* morphological changes are due to loss of LdcA activity. These studies also indicate that the *C. jejuni* LdcA ortholog, Pgp2, which is a putative periplasmic protein and lacks the Ser-Glu-His catalytic triad, exhibits LdcA activity in *F. tularensis*.

Deletion of FTL1678 affects sensitivity to antibiotics, detergents, and stressors

Given the above noted morphological differences in the Δ*FTL1678* envelope (*e.g.*, thicker OM; tightly-associated OM; more electron dense envelope structures) using TEM, we assessed envelope (*i.e.*, IM, PG, and OM) integrity by growing both WT and Δ*FTL1678* bacteria in the presence of various antibiotics, detergents, and dyes, and measuring zones of inhibition after 48 h of growth (Table 2). Δ*FTL1678* was found to be more susceptible than WT to ampicillin, vancomycin, lysozyme, and SDS (Table 2), indicating potential changes to PG (ampicillin sensitivity), OM integrity (vancomycin and lysozyme sensitivity), or efflux pumps

(SDS sensitivity). Conversely, Δ*FTL1678* was found to be more resistant than WT to gentamicin, tetracycline, chloramphenicol, ciprofloxacin, and ethidium bromide (Table 2). Given that the majority of these latter reagents must enter the cytoplasm to exert their inhibitory effects (*i.e.*, gentamicin, tetracycline, and chloramphenicol inhibit protein synthesis; ciprofloxacin and ethidium bromide interfere with DNA replication), these results suggest that Δ*FTL1678* bacteria exclude these inhibitory molecules from entering the cytoplasm.

To better understand potential differences in the Δ*FTL1678* envelope, WT and Δ*FTL1678* were grown in either sMHB at 37°C or in sMHB with various stress conditions. In sMHB at 37°C, Δ*FTL1678* did not exhibit a growth defect but, instead, appeared to grow to a higher optical density (OD_{600}) than WT (Figure 4A). However, as noted above, despite higher OD_{600} measurements for Δ*FTL1678* at several time points, bacterial numbers were not significantly different between WT and Δ*FTL1678* (Figure S5). Although speculative, the disassociation between Δ*FTL1678* optical densities and bacterial numbers may be due to the observed TEM morphological differences of Δ*FTL1678* (Figure 3 and Figure S6). Compared with growth in sMHB at 37°C, no substantial differences in the growth rates of WT and Δ*FTL1678* were observed at either 40°C (Figure 4B) or in the presence of 60 μM $CuCl_2$, an oxidizing agent (Ren, 2014); Figure 4C). However, Δ*FTL1678* grew considerably better than WT in the presence of 5 mM H_2O_2, 5% NaCl, and pH 5.5 (Figures 4D, 4E, and 4F, respectively), providing further evidence of modifications to the Δ*FTL1678* envelope. To confirm that Δ*FTL1678* envelope integrity differences were not due to polar effects, both the *FTL1678 trans*-complement and a *pgp2 trans*-complement were grown in the presence of the same stressors and both complemented strains were found to exhibit similar phenotypes as WT LVS (Figure S8A-D and Table S5). Taken together, these results indicated that loss of *FTL1678,* and its associated

LdcA activity, resulted in unidentified, and likely complex, perturbations in bacterial envelope components, including the OM, PG, and/or IM.

The Type A *F. tularensis* strain SchuS4 originally was isolated from a human tularemia patient and requires BSL3 containment. Given its relevance to human disease, we next generated an isogenic deletion mutant of the *FTL1678* homolog, *FTT0101*, in SchuS4. The susceptibilities of Δ*FTT0101* and WT SchuS4 to various antibiotics, detergents, and dyes were compared, with no significant differences observed (Table S6). At this time, we cannot fully explain why the Δ*FTL1678* mutant (*F. tularensis* Type B) displays altered sensitivity/resistance to antibiotics, detergents, and dyes (Table 2), while the Δ*FTT0101* mutant (*F. tularensis* Type A) did not demonstrate altered sensitivity/resistance toward these same compounds (compared to WT SchuS4; Table S6). However, this finding is not unexpected given genomic studies indicating that, despite >97% nucleotide identity between Type A and Type B *F. tularensis*, there are over 100 genomic rearrangements between Type A and Type B and each subspecies encodes over 100 unique genes that likely influence known differences in Type A and Type B virulence (Petrosino *et al.*, 2006).

FTL1678 and LdcA activity are required for F. tularensis virulence in vivo

To examine if FTL1678 plays a role in *F. tularensis* virulence, groups of C3H/HeN mice were intranasally infected with 10^4 CFU of either WT or Δ*FTL1678* and monitored daily for signs of disease. Whereas all WT-infected mice died by day 9 post-infection (median time-to-death day 6), Δ*FTL1678* was completely attenuated (100% survival through day 21 post-infection), demonstrating that FTL1678 is required for *F. tularensis* virulence (Figure 5A). To confirm that the observed attenuation was solely due to the deletion of *FTL1678*, and not to polar

effects, we tested the virulence of the Δ*FTL1678 in trans*-complement in mice, which fully-restored virulence to WT levels (all mice died by day 7; median time-to-death day 6; Figure 5A).

To more carefully assess Δ*FTL1678* attenuation *in vivo*, we intranasally-infected mice with 10^4 CFU of either WT LVS or Δ*FTL1678*, and enumerated bacterial CFUs from lungs, livers, spleens, and blood on days 2 and 5 post-infection to examine bacterial replication and dissemination to these organs/tissues over time. On day 2 post-infection, WT LVS replicated to $>10^7$ CFU/mg lung and had disseminated to livers, spleens (approx. 10^3 CFU/mg), and blood (10^3 CFU/ml; Figure 5B). In contrast, Δ*FTL1678* had an initial (day 2) colonization defect in the lungs (>35,000-fold lower than WT) and was unable to disseminate to livers, spleens, or blood (Figure 5B). By day 5 post-infection, the attenuation of Δ*FTL1678* was even more apparent, with WT LVS replicating to extremely high numbers (approx. 10^8 CFU/mg) in lungs, livers, and spleens, compared with Δ*FTL1678*, which replicated in lungs between day 2 and 5, but was >11,000-fold attenuated in lungs and was not detectable in livers or spleens (Figure 5B). Although Δ*FTL1678* was detected in the blood on day 5, it was 142-fold less than WT LVS (Figure 5B).

As noted above, of the six Ldc orthologs examined here, only *C. jejuni* Pgp2 lacks the Ser-Glu-His catalytic triad (Figure 1). However, *C. jejuni* Pgp2 has been shown to exhibit LdcA activity (Frirdich, 2014), indicating that a Ser-Glu-His catalytic triad is not required for LdcA function. To test if an LdcA ortholog, without the Ser-Glu-His catalytic triad, could restore virulence in the Δ*FTL1678* mutant, we complemented Δ*FTL1678* with *C. jejuni* Pgp2 *in trans* and infected groups of mice with either WT LVS, Δ*FTL1678*, Δ*FTL1678 trans*-complemented with FTL1678, or Δ*FTL1678 trans*-complemented with *C. jejuni* Pgp2. While Δ*FTL1678* was fully attenuated (100% survival through day 21), the Pgp2 *trans*-complement was fully-virulent

(median time-to-death 6 days; all mice dead by day 7), nearly identical to WT LVS (median time-to-death 7 days; all mice dead by day 7) and the FTL1678 *trans*-complement (median time-to-death 6 days; all mice dead by day7; Figure 5C). These *in vivo* data provide further evidence that FTL1678 is an Ldc and that Ldc activity, with or without the Ser-Glu-His catalytic triad, is required for *F. tularensis* virulence.

Finally, given the relevance of SchuS4 to human disease, we next examined the virulence of Δ*FTT0101*, the *FTL1678* homolog, in our mouse infection model. When groups of C3H/HeN mice were intranasally-infected with either WT SchuS4 or Δ*FTT0101*, all mice died by day 7 post-infection, indicating that *FTT0101* is not required for SchuS4 virulence (Figure S9). Whereas Δ*FTT0101*-infected mice exhibited a slightly delayed time-to-death (median time-to-death day 6; Figure S9), compared with WT SchuS4-infected mice (median time-to-death day 5; Figure S9), this may be due to differences in the infectious dose administered to mice in this experiment (80 CFU SchuS4; 12 CFU Δ*FTT0101*). However, it also remains possible that the extreme virulence of SchuS4 (intranasal LD_{50} <10 CFU in our hands) and over 100 genomic rearrangements between Type A and Type B *F. tularensis* (noted above) complicates assessments of mutant attenuation *in vivo*.

Individual residues of the FTL1678 catalytic triad are not required for F. tularensis virulence in vivo

As noted above and highlighted in Figure 1, *P. aeruginosa* LdcA contains a Ser-Glu-His catalytic triad which is essential for function and is characteristic of Ldc in the Peptidase_S66 family (Korza, 2005). The same catalytic triad also has been confirmed in Ldc from *E. coli* (Meyer, 2018), *Novosphingobium aromaticivorans* (Das, 2013), and *N. gonorrhoeae* (Lenz,

2017). Given the relatively conserved spacing of Ser134-Glu239-His308 residues in FTL1678 (Figure 1) and our findings that both double (S134A/E239A, S134A/H308A, E239A/H308A) and triple (S134A/E239A/H308A) mutants did not exhibit LdcA activity (Table S3), we tested if individual amino acid residues of the catalytic triad were required for *F. tularensis* virulence (similar to Figure 5A virulence assessments for Δ*FTL1678* and the FTL1678 complemented strain). Site-directed mutagenesis was performed to independently generate FTL1678 complementation constructs containing either S134A, E239A, or H308A mutations. Next, Δ*FTL1678* was complemented *in-trans* with each of these FTL1678 catalytic triad point mutants, and groups of C3H/HeN mice were intranasally infected with either WT, Δ*FTL1678*, Δ*FTL1678* *trans*-complemented with *FTL1678*, or Δ*FTL1678* *trans*-complemented with one of the FTL1678 catalytic triad point mutants (referred to hereafter as S134A, E239A, and H308A). Confirming our previous findings, Δ*FTL1678* was completely attenuated (100% survival through day 21), while complementation of Δ*FTL1678* with either FTL1678 (all mice dead by day 8), S134A (all mice dead by day 7), E239A (all mice dead by day 8), or H308A (all mice dead by day 8), fully-restored virulence to WT LVS levels (all mice dead by day 10; Figure S10). These results should not be overinterpreted, as it is difficult to directly compare or fully explain why mutations of single amino acids in the FTL1678 putative catalytic triad had no effect on *in vivo* virulence (Figure S10), while mutations of any two amino acids in the catalytic triad ablated FTL1678 LdcA enzyme activity *in vitro* (Table S3). It remains possible that single or multiple residues of the FTL1678 catalytic triad are required for full LdcA activity *in vitro* or that, in the context of the whole bacterium (*i.e., in vivo*), other *F. tularensis* proteins may have compensated for partially-functional FTL1678, due to S134A, E239A, and H308A single amino acid mutations. Regardless, these studies indicate that, while single amino acid mutations of the

FTL1678 Ser-Glu-His catalytic triad do not impact *F. tularensis* virulence *in vivo*, two or more residues of the Ser-Glu-His catalytic triad are required for *FTL1678* LdcA activity.

FTL1678 is required for F. tularensis replication in macrophages

F. tularensis is an intracellular pathogen and macrophages appear to be one of the major targets for *F. tularensis* infection and replication (De Pascalis, 2018, Steiner, 2017, Hall, 2008). To investigate potential replication defects of Δ*FTL1678* in macrophages, J774A.1 macrophages or murine bone marrow-derived macrophages (mBMDM) were infected with either WT LVS or Δ*FTL1678* (MOI 100:1) and bacterial numbers were enumerated at 0 h (entry), 6 h, and 24 h post-infection. At entry (0 h), > 300-fold more Δ*FTL1678* were present in both macrophage lines, compared with WT LVS (Figure 6A). This likely was due to the above noted gentamicin resistance of Δ*FTL1678* (Table 2). Attempts to normalize entry numbers for both WT LVS and Δ*FTL1678*, using different antibiotics or combinations of antibiotics, were not successful. Despite higher numbers of Δ*FTL1678* in both macrophages at entry (0 h) and 6 h, Δ*FTL1678* was unable to replicate in either macrophage, decreasing 13-fold in BMDM and 5-fold in J774A.1 macrophages from 6 h to 24 h (CFU data in Figure 6A; fold change data in Figure 6B). By comparison, WT LVS numbers increased 236-fold in BMDM and 22-fold in J774A.1 macrophages from 6 h to 24 h (Figure 6A-B). Taken together, these *in vitro* results (Figure 6A-B) confirm the observed *in vivo* attenuation of Δ*FTL1678* (Figure 5A-C).

ΔFTL1678 protects mice against Type A F. tularensis infection

No FDA-approved vaccine currently is available to prevent tularemia. In addition, *F. tularensis* is designated as an NIH Category A priority pathogen and CDC Tier 1 Select Agent,

highlighting the extreme virulence of this bacterium and the need for a safe and effective vaccine to prevent tularemia. Given our above findings that 10^5 CFU of Δ*FTL1678* did not cause disease or death in mice (Figure 5A-C), we next examined whether high doses (10^7 or 10^9 CFU) of Δ*FTL1678* were attenuated or if Δ*FTL1678* immunization could protect mice from fully-virulent Type A *F. tularensis* SchuS4 challenge. First, all mice intranasally immunized with either 10^5, 10^7, or 10^9 CFU of Δ*FTL1678* survived through day 28 post-infection, with no signs of clinical disease (Figure 7A). Next, on day 29, all mice were boosted with 10^9 CFU of Δ*FTL1678* and no mice demonstrated any signs of disease through day 50 (Figure 7A). Finally, on day 51, mice were intranasally-challenged with 120 CFU (6× the LD_{50}) of SchuS4 and the health status of each immunization group was monitored for 26 days post-challenge. In a dose-dependent manner, the 10^9 prime-10^9 boost regimen conferred 80% protection, the 10^7 prime-10^9 boost regimen conferred 40% protection, and the 10^5 prime-10^9 boost regimen conferred 20% protection (Figure 7B). These data demonstrate that Δ*FTL1678* is highly attenuated (up to 10^9 CFU) and that Δ*FTL1678* may be able to be used as a live, attenuated vaccine.

ΔFTL1678 does not cause tissue damage

The *in vitro* (Figure 6) and *in vivo* (Figure 5A-C and Figure 7A) attenuation of Δ*FTL1678*, as well as protection against SchuS4 pulmonary challenge (Figure 7B), indicated that Δ*FTL1678* could be used as a live, attenuated vaccine. While live, attenuated vaccines have been extremely effective at preventing a number of diseases, they can pose safety challenges (Minor, 2015, Roberts, 2018). To assess whether Δ*FTL1678* immunization induced any pathology in immunized mice, lungs, livers, and spleens from uninfected, WT LVS-, or Δ*FTL1678*-infected mice were assessed for pathologic changes on day 5 post-

483 infection/immunization. Day 5 is when mice exhibit severe signs of disease and is one day
484 before the majority of WT-infected mice begin succumbing to disease (Figures 5 and 7). WT
485 LVS-infected lungs demonstrated alveolar wall thickening, large areas of inflammation, and
486 severe neutrophil infiltration (Figure 8A). By comparison, little inflammation was observed in
487 Δ*FTL1678*-infected lungs, although some red blood cell congestion was present, indicating a
488 limited, acute immune response that was quickly resolved (Figure 8A). Whereas WT LVS-
489 infected livers were characterized by diffuse inflammation with focal areas of necrosis,
490 Δ*FTL1678*-infected livers were virtually indistinguishable from uninfected livers, with no
491 observable pathology (Figure 8A). Finally, although the architecture of WT LVS-infected
492 spleens lacked distinct areas of white pulp or red pulp, indicative of a severe infection,
493 Δ*FTL1678*-infected spleens were observed to contain distinct areas of red pulp and white pulp,
494 with some red blood cell congestion – indicating a limited, acute immune response that was
495 quickly resolved (Figure 8A). All tissues were blindly scored using a pathology severity index
496 (scale from 0 to 4, with 4 indicating severe pathology), confirming that Δ*FTL1678*-infected
497 tissues were virtually indistinguishable from uninfected tissues (pathology scores of 1 for lungs,
498 0 for liver, and 1.5 for spleens) and WT LVS-infected tissues had significantly higher pathology
499 scores (pathology scores >3.5 for all tissues; Figure 8B).
500
501 **Discussion**
502 Bacterial PG is a complex, mesh-like structure, composed of a glycan backbone,
503 crosslinked to varying degrees, by peptide chains (de Pedro, 2015). It is well known that this
504 structure plays an important role in maintaining Gram-negative bacterial cell morphology,
505 membrane integrity, regulating changes in osmotic pressure, and providing a platform for

attachment of the OM (den Blaauwen, 2008, Silhavy *et al.*, 2010). Although a majority of PG studies have focused on how the thick layer of PG in Gram-positive bacteria contributes to virulence and antibiotic resistance, more recent studies have highlighted that Gram-negative PG also is intimately linked with pathogenicity (Juan, 2018).

PG recycling is an essential function of Gram-negative bacteria during cell growth and division to produce new cell wall components. In fact, Gram-negative bacteria recycle up to 60% of their PG with every generation, suggesting that both PG synthesis and PG recycling are dynamic (Dhar, 2018, Typas, 2011, Park, 2008). A number of proteins are involved in these processes and, while they are well-characterized in *E. coli*, very little is known about these pathways in intracellular pathogens such as *Burkholderia pseudomallei*, *Legionella pneumophila*, or *F. tularensis* (van Heijenoort, 2011, Jenkins, 2019, Spidlova, 2018, Kijek, 2019).

E. coli LdcA, a cytoplasmic protein, was the first L,D-carboxypeptidase to be identified and was shown to be important for PG recycling and survival during stationary phase (Ursinus, 1992, Templin, 1999). More recently, Ldc orthologs have been identified in *P. aeruginosa* (Korza, 2005), *C. jejuni* (Frirdich, 2014), *N. gonorrhoeae* (Lenz *et al.*, 2017), and *N. aromaticivorans* (Das, 2013). In this study, we identified an *F. tularensis* Ldc ortholog, FTL1678, which we propose naming LdcA based on its confirmed L,D, carboxypeptidase activity (Table 1) and role in maintaining bacterial morphology. Unlike well-characterized cytoplasmic LdcA orthologs from *E. coli* and *P. aeruginosa*, we demonstrated that *F. tularensis* LdcA was localized to OM fractions and, given co-localization with PG-associated proteins Pal and TolB, is most likely located on the inner leaflet of the OM or in the periplasm (associated with PG). At this time, we can only speculate on the OM-association or periplasmic localization

of *F. tularensis* LdcA, but in the context of PG repair and recycling, periplasmic LdcA certainly offers a fitness advantage. In addition, this is not the first report of a periplasmic LdcA, as *C. jejuni* Pgp2 is predicted to be periplasmic and *N. gonorrhoeae* LdcA previously was reported to be periplasmic (Lenz, 2017, Frirdich, 2014).

Our results demonstrated, for the first time, that *F. tularensis* LdcA directly acts on the TCT tetrapeptide and the reducing PG monomer. More importantly, we demonstrated that *F. tularensis* LdcA directly cleaves PG pentapeptides to tripeptides, without a prior cleavage event by a D,D-carboxypeptidase/penicillin binding protein (PBP), such as DacD, and that FTL1678 cleaves TCT dimers with 4-3 and 3-3 cross links, highlighting that *F. tularensis* LdcA is a multi-functional enzyme that exhibits both L,D-carboxypeptidase and L,D-endopeptidase activities (Table 1 and Table S2). It should be noted that although *N. gonorrhoeae* LdcA also has been reported to have L,D-endopeptidase activity, this activity was shown to cleave tetra-tri and tri-tri dimers, but not tetra-tetra dimers, suggesting a specificity for 3-3 cross linked dimers (Lenz, 2017). Interestingly, only two previous studies have examined putative *F. tularensis* PG modifying enzymes and both studies primarily focused on the role of an *F. tularensis* DacD ortholog in virulence, with no PG activity assays to confirm function (Spidlova, 2018, Kijek, 2019). In our PG cleavage analysis, *F. tularensis* LdcA demonstrated the highest specific activity on disaccharide-tetrapeptide PG substrates (GlcNAc-anhydroMurNAc-L-Ala-γ-D-Glu-*meso*-A_2pm-D-Ala [TCT] and GlcNAc-MurNAc-L-Ala-γ-D-Glu-*meso*-A_2pm-D-Ala [reducing PG monomer]), followed by cleavage of pentapeptide PG substrates (MurNAc-L-Ala-γ-D-Glu-*meso*-A_2pm-D-Ala-D-Ala and UDP-MurNAc-L-Ala-γ-D-Glu-*meso*-A_2pm-D-Ala-D-Ala). Despite high specific activity of *F. tularensis* LdcA on tetrapeptide attached to the disaccharide, *F. tularensis* LdcA demonstrated approximately 6-times lower specific activity on free

552 tetrapeptide (no sugars) (Table 1). In contrast, *E. coli* LdcA has been shown to have the highest
553 specific activity on free tetrapeptide, monosaccharide-tetrapeptide (MurNAc-L-Ala-γ-D-Glu-
554 *meso*-A_2pm-D-Ala), and monosaccharide tetrapeptide linked to a glycan lipid carrier (UDP-
555 MurNAc-tetrapeptide) (Templin, 1999), but is unable to cleave dimeric muropeptides.
556 Additionally, *F. tularensis* LdcA was active against different forms of dimers (two TCT
557 monomers carrying tri- or tetrapeptide chains connected either by a 4-3 or a 3-3- crosslink) but
558 was not active on the PG polymer. The cleavage of the latter dimers indicated that *F. tularensis*
559 LdcA possesses both L,D-endopeptidase and L,D,-carboxypeptidase activities and could cleave
560 the A_2pm-A_2pm, A_2pm-D-Ala and A_2pm-Gly peptide bonds (L-D bonds in all cases) present in
561 these dimers, with more or less efficacy.

562 Previous studies have shown that Ldc orthologs are important for bacterial morphology
563 and membrane integrity. Deletion of the *ldc* orthologs *csd6* from *H. pylori* (Sycuro, 2013) and
564 *pgp2* from *C. jejuni* (Frirdich, 2014) resulted in loss of helical morphology. Here, we
565 demonstrated that FTL1678 is essential for maintaining both the size (width) and the
566 coccobacillus morphology of *F. tularensis,* as Δ*FTL1678* bacteria were significantly-smaller
567 than WT and exhibited a more-rounded, cocci shape than WT (Figure 3). Further evidence for
568 the role of *F. tularensis* LdcA in modifying and recycling PG, which impacts bacterial
569 morphology, is provided by TEM images of Δ*FTL1678* bacteria that have prominent three-
570 layered structures at their periphery, including a thick middle layer (presumably PG), compared
571 to WT (Figure 3). In Δ*FTL1678* bacteria, it is possible that loss of LdcA activity may have
572 reduced PG recycling or may have affected the breakdown of existing PG (important for cell
573 division), resulting in a buildup of pentapeptides or tetrapeptides that are highly-crosslinked.
574 Our lab and others have repeatedly attempted to isolate and analyze *F. tularensis* PG but theses

attempts have not been successful. As such, we can only speculate on the true nature of the thick PG and OM layers in Δ*FTL1678* (Figure 3).

Because Δ*FTL1678* bacteria were found to have a thicker OM (Figure 3C), a prominent middle layer in their envelope (presumably PG; Figure 3B), and an altered cell morphology (Figure 3B), we investigated differences in WT and Δ*FTL1678* susceptibility to various antibiotics, detergents, and stressors. Vancomycin and lysozyme, usually not effective against Gram-negative species due to their inability to penetrate the OM, inhibited Δ*FTL1678* growth (Table 2), indicating increased permeability of the Δ*FTL1678* OM. Vancomycin, in particular, may have been effective on Δ*FTL1678* because its mechanism of action includes binding to the two terminal D-Ala-D-Ala residues of PG pentapeptide chains and preventing cross-linking of monomers. Δ*FTL1678* may have increased amounts of pentapeptides present in its PG, providing more targets for vancomycin action. Similarly, ampicillin inhibits bacterial transpeptidases, which blocks cross-linking of peptide side chains of PG strands. Taken together, the enhanced susceptibility of Δ*FTL1678* bacteria to vancomycin and ampicillin supports the role of *F. tularensis* LdcA as a PG-modifying enzyme. Conversely, Δ*FTL1678* was more resistant to antibiotics and molecules that must cross the IM to exert their toxic effects, including gentamicin, tetracycline, chloramphenicol, ciprofloxacin, and ethidium bromide (Table 2), suggesting that Δ*FTL1678* bacteria have a less permeable IM. Indeed, decreased permeability of the IM and altered activity of IM efflux pumps may help explain the more electron-dense staining of Δ*FTL1678*, compared to WT (Figure 3). Many mechanisms may explain why Δ*FTL1678* bacteria were more resistant to other stressors, including H_2O_2, high salt, and low pH, including increased expression/activity of chaperone proteins, efflux pumps, antioxidant/scavenger proteins, and membrane stabilizing proteins (Mishra & Imlay, 2012,

598 Knodler *et al.*, 2003, Lund *et al.*, 2014). Future studies are needed to define these mechanisms,
599 which are likely to be complex.

600 The extreme virulence of Type A *F. tularensis* and its designation as a Tier 1 Select
601 Agent highlight why studies to identify *F. tularensis* virulence factors and the development of
602 new vaccines is important. In this study, we identified the role of a previously unstudied protein,
603 FTL1678, in PG recycling, PG integrity, and bacterial morphology. In addition, we found that
604 FTL1678 was required for *F. tularensis* LVS virulence and demonstrated that Δ*FTL1678*
605 conferred 80% protection against fully-virulent, Type A *F. tularensis* SchuS4 pulmonary
606 challenge. Further studies are needed to determine specific immune responses induced by
607 Δ*FTL1678* immunization, as well as to identify the most effective immunization regimen (*e.g.,*
608 number of immunizations and time between immunizations).

609 Finally, given our findings that PG maintenance and recycling are important for *F.*
610 *tularensis* virulence, and that future studies may reveal additional PG-associated enzymes, we
611 used bioinformatic approaches to predict other proteins involved in *F. tularensis* PG synthesis
612 and recycling (Figure 9). While at least seven PG synthesis and recycling genes/proteins
613 orthologs could not be identified, 22 putative PG synthesis and recycling proteins were identified
614 in *F. tularensis* (Figure 9). Of these, only DacD (FTL1060/FTT1029) has been studied in *F.*
615 *tularensis*. Given our observed attenuation of Δ*FTL1678*, future studies to better understand PG
616 synthesis and recycling pathways may offer more opportunities to better understand the virulence
617 of *F. tularensis* and other intracellular pathogens. Characterization of other proteins involved in
618 PG pathways may provide clues as to why *F. tularensis* LdcA is OM-associated or periplasmic
619 and encodes both L,D-carboxypeptidase and L,D-endopeptidase activities.
620

Experimental Procedures

Bacterial strains and culture conditions

F. tularensis Type A strain SchuS4 and *F. tularensis* Type B strain LVS were obtained from BEI Resources and cultured as previously described (Wu, 2016, Ren, 2014). All experiments with SchuS4 were performed under BSL3 containment conditions at the University of Toledo Health Science Campus BSL3 laboratory. Routine *F. tularensis* cultures were grown overnight at 37°C with 5% CO_2 on supplemented Mueller-Hinton agar (sMHA): Mueller-Hinton broth powder (Becton Dickinson) was mixed with 1.6% (wt/vol) Bacto Agar (Becton Dickinson), autoclaved, and further supplemented with 2.5% (vol/vol) bovine calf serum (Hyclone), 2% (vol/vol) IsoVitaleX (Becton Dickinson), 0.1% (wt/vol) glucose, and 0.025% (wt/ vol) iron pyrophosphate. For mouse infections, *F. tularensis* was first grown on sMHA then transferred to Brain Heart Infusion agar (BHI; Becton Dickinson). Chocolate agar for mutant strain generation was prepared by mixing Mueller-Hinton broth powder with 1.6% (wt/vol) agar, 1% (wt/vol) tryptone, and 0.5% (wt/vol) sodium chloride, autoclaved, and further supplemented with 1% (wt/vol) hemoglobin and 1% (vol/vol) IsoVitaleX. For macrophage infections, *F. tularensis* was first grown on sMHA then transferred to modified chocolate agar: Mueller-Hinton broth powder was mixed with 1.6% (wt/vol) Bacto Agar, 1% hemoglobin (wt/vol), and 1% (vol/vol) IsoVitaleX. All growth curves were performed in sMHB: Mueller-Hinton broth powder was mixed with 182 µg ml^{-1} calcium chloride dihydrate, and 210 µg ml^{-1} magnesium chloride hexahydrate, 0.1% (wt/vol) glucose, 0.025% (wt/vol) iron pyrophosphate, and 2% (vol/vol) IsoVitaleX. All bacterial strains and plasmids are listed in Table S7. *E. coli* S17-1 and *E. coli*

NEB10-β were grown in Luria Bertani (LB) broth or on LB agar at 37°C, supplemented as needed with antibiotics.

Sequence alignments and bioinformatic predictions

Amino acid alignments of *F. tularensis* subsp. *holarctica* FTL_1678, *F. tularensis* subsp. *tularensis* FTT_0101, *E. coli* LdcA (BAA36050.1), *P. aeruginosa* LdcA (Q9HTZ1), *N. gonorrhoeae* LdcA (YP_208343.1), and *C. jejuni* Pgp2 (WP_002856863) were performed using Clustal Omega (https://www.ebi.ac.uk/Tools/msa/clustalo/) and MView (https://www.ebi.ac.uk/Tools/msa/mview/). Pairwise sequence alignments were performed and amino acid identities among Ldc homologs were calculated by EMBOSS Needle (https://www.ebi.ac.uk/Tools/psa/emboss_needle/). The Prokaryotic Genome Analysis Tool (PGAT) (http://tools.uwgenomics.org/pgat/), BlastP, and BlastX analyses (http://blast.ncbi.nlm.nih.gov) were used to identify *F. tularensis* homologues. Bacterial protein sub-localization was predicted by PSORTb version 3.0.2 (https://www.psort.org/psortb/). Protein signal sequence prediction was performed by LipoP version 1.0 (http://www.cbs.dtu.dk/services/LipoP/) and SignalP version 4.1 (http://www.cbs.dtu.dk/services/SignalP-4.1/).

Expression and purification of recombinant FTL1678 and FTT0101

F. tularensis LVS and SchuS4 genomic DNA were extracted using phenol/chloroform/isoamyl alcohol (Fisher Bioreagents). *FTL1678* and *FTT0101*, without signal sequences (amino acid residues 1-29), were PCR-amplified from LVS and SchuS4 genomic DNA, respectively, using High Fidelity Platinum Taq Polymerase (Life Technologies), and primers 5'FTL1678_BamHI

and 3'FTL1678_XhoI and 5'FTT0101_BamHI and 3'FTT0101_XhoI, respectively (Table S8). Amplicons and pPROEX HTb were double-digested with BamHI and XhoI, ligated using T4 DNA ligase, and transformed into NEB 10-β *E. coli*. Plasmids were purified using the Qiagen QIAprep Spin Miniprep kit and diagnostic PCR was performed to confirm presence and correct size of the insert. DNA sequencing was performed to confirm insert integrity and plasmid constructs were transformed into Rosetta DE3 *E. coli* (Millipore) for protein expression. Recombinant proteins were expressed and purified as previously described (Ren, 2014) with some modifications. Bacteria were grown in LB-amp to an OD_{600} of 0.4, protein expression was induced for 2 h by the addition of isopropyl β-D-thiogalactopyranoside (IPTG) to a final concentration of 100 µM, bacteria were pelleted by centrifugation, and frozen overnight at -80°C to aid in lysis. Cell pellets were suspended in 10 mM Tris, 500 mM NaCl, and 10 mM imidazole, pH 8.0, sonicated on ice for 10 min with 30 sec intervals, insoluble material was removed by centrifugation at 8,000 × *g*, and supernatants were collected for affinity purification over pre-equilibrated nickel-nitrilotriacetic acid (Ni-NTA) agarose (Qiagen) columns. Eluted recombinant proteins were concentrated in Amicon Ultra-4 centrifugal filter units with 30-kDa cutoff (Millipore), concentrations were determined using the DC BCA protein assay (BioRad), and purity was assessed by SDS-PAGE and Imperial protein staining (Thermo Scientific). An empty vector construct also was expressed and purified as a control in enzymatic assays.

Site-directed mutagenesis of recombinant FTL1678

The QuikChange Lightning site-directed mutagenesis kit (Agilent) was used to generate single amino acid, double amino acid, and triple amino acid mutations in the FTL1678 putative active site residues S134, E239, and H308. Three separate QuikChange reactions were performed in a

thermocycler using purified plasmid DNA from pFNLTP6-gro-*flt1678*-6xHis and three primer sets to individually mutate Ser134 to Ala (S134A), Glu239 to Ala (E239A), and His308 to Ala (H308A): a400g_g401c_5' and a400g_g401c_3'(S134), a716c_5' and a716c_3' (E239), and c922g_a923c_5' and c922g_a923c_3'(H308) (Table S8). Following amplification, products were digested with DpnI and immediately transformed into NEB 10-β *E. coli*. Transformants were selected on LB-kan overnight, plasmids were purified for individual clones, and DNA sequencing was performed to confirm individual mutations. The resulting plasmids were named pFNLTP6-gro-*ftl1678*-S134A-6xHis, pFNLTP6-gro-*ftl1678*-E239A-6xHis, and pFNLTP6-gro-*ftl1678*-H308A-6xHis (Table S7). To generate the catalytic triad point mutant complement strains, S134A, E239A, and H308A, pFNLTP6-gro-*ftl1678*-S134A-6xHis, pFNLTP6-gro-*ftl1678*-E239A-6xHis, and pFNLTP6-gro-*ftl1678*-H308A-6xHis were individually transformed into kan-cured Δ*FTL1678* by electroporation, transformants were selected on sMHA-kan10, and expression of S134A, E239A, and H308A were confirmed by immunoblot analysis. To generate double and triple active site mutants for recombinant protein expression, three separate QuikChange reactions were performed using purified plasmid DNA from pPROEX Htb-FTL1678 as described above, using the same three primer sets to mutate S134, E239, and H308. DNA sequencing was performed to confirm individual mutations. Plasmids were named pPROEX Htb-*ftl1678*-S134A, pPROEX Htb-*ftl1678*-E239A, and pPROEX Htb-*ftl1678*-H308A (Table S7). Three separate QuikChange reactions were performed as described above to generate double mutants. Purified plasmid DNA from pPROEX Htb-*ftl1678*-S134A was amplified with a716c_5' and a716c_3' to generate an S134A/E239A double mutant and separately with c922g_a923c_5' and c922g_a923c_3' to generate an S134A/H308A double mutant. Purified plasmid DNA from pPROEX Htb-*ftl1678*-E239A was amplified with

c922g_a923c_5' and c922g_a923c_3' to generate an E239A/H308A double mutant. Transformants were selected on LB-kan overnight, plasmids were purified for individual clones, and DNA sequencing was performed to confirm double mutations. The resulting plasmids were named pPROEX Htb-*ftl1678*-S134A/E239A, pPROEX Htb-*ftl1678*-S134A/H308A, and pPROEX Htb-*ftl1678*-E239A/H308A. A final QuikChange reaction was performed to generate the triple active site mutant, S134A/E239A/H308A. Purified plasmid DNA from pPROEX Htb-*ftl1678*-S134A/E239A was amplified using the primer set c922g_a923c_5' and c922g_a923c_3', transformants were selected on LB-kan overnight, plasmids were purified for individual clones, DNA sequencing was performed to confirm the triple mutation and the plasmid was named pPROEX Htb-*ftl1678*-S134A/E239A/H308A (Table S7). All four plasmid constructs were transformed into Rosetta DE3 *E. coli* for protein expression. Recombinant proteins were expressed and purified as described above.

Enzymatic assays for FTL1678/FTT0101 activity

FTL1678 and FTT0101 recombinant protein activities toward various PG-related compounds were tested in 50 µl reaction mixtures containing 50 mM Tris-HCl, pH 8.0, 0.1 mM substrate, and partially purified enzyme stock (10 µl in 1 M NaCl, 10 mM Tris, pH 8.0). Mixtures were incubated at 37°C and reactions were stopped by freezing. Depending on the substrate used, the amount of partially purified protein varied from 0.9 to 5 µg per assay and incubation time varied from 30 min to 4 h. Substrate and reaction products were separated by HPLC on an ODS-Hypersil 3 µm particle-size C18 column (250 × 4.6 mm; Thermo Scientific). Elutions were performed with 50 mM sodium phosphate buffer, pH 4.5, with or without application of a linear gradient of methanol (from 0 to 20% in 80 min), at a flow rate of 0.5 ml/min. Peaks were

735 detected by measuring the absorbance at 207 nm or at 262 nm for UDP-containing nucleotide
736 precursors. Identification of reaction products was based on their retention times, compared to
737 authentic standards, as well as on their amino acid and amino sugar composition, determined
738 with a Hitachi model L8800 analyzer (Sciencetec) after hydrolysis of samples in 6 M HCl for 16
739 h at 95°C. Enzyme activity was calculated by integration of peaks corresponding to the
740 substrates and products. To ensure linearity, substrate consumption was < 20% in all cases. The
741 amounts of D-Ala and D-Ala-D-Ala released during the reactions also were determined by
742 injection of aliquots of these reaction mixtures in the Hitachi amino acid analyzer. FTL1678
743 double and triple active site mutants were tested using the same conditions, with the incubation
744 time being prolonged up to 18h.
745
746 *Peptidoglycan precursors and muropeptides*
747 UDP-MurNAc-pentapeptide precursors containing either *meso*-diaminopimelic acid (A_2pm) or
748 L-lysine were prepared by enzymatic synthesis using purified Mur ligases, and UDP-MurNAc-
749 tetrapeptides were generated by treatment of the UDP-MurNAc-pentapeptide precursors with
750 purified *E. coli* PBP5 DD-carboxypeptidase as previously described (Herve, 2007). MurNAc-
751 peptides were obtained by mild acid hydrolysis of UDP-MurNAc-peptides (0.1 M HCl, 100°C,
752 15 min) and were not reduced and thus purified as a mixture of the two α and β anomers (Blanot,
753 1983). Free peptides were prepared by cleavage of MurNAc-peptides with *E. coli* AmiD *N*-
754 acetylmuramoyl-L-alanine amidase (Pennartz, 2009). The *E. coli* peptidoglycan polymer was
755 purified from a Δ*lpp* mutant strain that does not express the Lpp lipoprotein (Leulier, 2003).
756 GlcNAc-1,6-anhydro-MurNAc-L-Ala-γ-D-Glu-*meso*-A_2pm-D-Ala (TCT) and its dimer (two
757 cross-linked TCT monomers) were produced by digestion of peptidoglycan with *E. coli* SltY

lytic transglycosylase and the non-anhydro forms of these monomer and dimer were generated by digestion of the polymer with mutanolysin (Stenbak, 2004). All these compounds were HPLC-purified (Table S1) and their composition was controlled by amino acid and amino sugar content analysis and/or by MALDI-TOF mass spectrometry.

Generation of F. tularensis gene deletion mutants

F. tularensis isogenic deletion mutants were generated by homologous recombination as previously described (Wu, 2015). Briefly, 500-bp regions upstream and downstream from the gene of interest (*FTL1678* or *FTT0101*) were PCR-amplified from *F. tularensis* genomic DNA using the following primers: FTL1678_A and FTL1678_B; FTL1678_C and FTL1678_D; FTT0101_A and FTT0101_B; FTT0101_C and FTT0101_D (Table S8). A FLP recombination target (FRT)-flanked Pfn-kanamycin resistance cassette, FRT-Pfn-kan-FRT, was PCR amplified from pLG66a (Gallagher, 2008) and splicing overlap extension PCR (SOE PCR) was used to join the upstream (A-B) and downstream (C-D) regions with FRT-Pfn-kan-FRT, which replaced the gene of interest. The resulting insert and a suicide plasmid, pTP163 (Robertson, 2013), were digested with ApaI (New England Biolabs), and ligated using T4 DNA ligase (New England Biolabs). Gene deletion constructs were transformed into NEB10-β *E. coli* (New England Biolabs), sequence-verified, transformed into *E. coli* S17-1, and conjugation was performed with *F. tularensis* LVS on sMHA plates. Conjugants were recovered on chocolate agar supplemented with 200 µg ml^{-1} hygromycin and 100 µg ml^{-1} polymyxin B. Individual mutants were selected by sequential plating on sMHA supplemented with 10 µg ml^{-1} kanamycin (sMHA-kan10), sMHA-kan10 with 8% (wt/vol) sucrose, and final replica plating onto sMHA containing either

200 µg ml^{-1} hygromycin (sMHA-hyg200) or sMHA-kan10. Hyg-sensitive and kan-resistant colonies were sequence verified (referred to hereafter as either Δ*FTL1678* or Δ*FTT0101*).

FTL1678 complementation in trans

Complementation *in trans* was performed as previously described, with some modifications (Wu, 2016). *FTL1678* was PCR-amplified from *F. tularensis* LVS using primers 5'FTL1678_NEBuilder and 3'FTL1678_NEBuilder (Table S8), pQE-60 (Qiagen) was double-digested with NcoI and BglII (New England Biolabs), and the NEBuilder HiFi DNA Assembly Cloning kit was used to ligate the *FTL1678* amplicon and digested pQE-60. The construct was transformed into NEB 10-β *E. coli* and transformants were selected on LB agar supplemented with 100 µg ml^{-1} ampicillin (LB-amp). Plasmids were purified from individual clones using the Qiagen QIAprep Spin Miniprep kit (Qiagen), diagnostic PCR was performed to confirm insert presence and correct size, and DNA sequencing was performed to verify insert integrity. The resulting construct, *FTL1678* with a C-terminal 6×histidine tag, was PCR-amplified using primers 5'FTL1678_pFNLTP6 and 3'FTL1678_pFNLTP6 (Table S8), the amplicon and pFNLTP6-gro-GFP (Maier, 2004) were double-digested with XhoI and BamHI (New England Biolabs), and ligated using T4 DNA ligase. The construct, pFNLTP6-gro-*FTL1678*-6xHis, was transformed into NEB10-β *E. coli*, transformants were selected on LB plates supplemented with 50 µg ml^{-1} kanamycin (LB-kan), and DNA sequencing was performed to verify FTL1678-6xHis integrity. Next, the kan resistance gene was removed from Δ*FTL1678* by suspending the strain in 0.5 M sucrose (in 1 mM EDTA, pH 7.5), washing three times, and electroporating the shuttle plasmid pTP405 (Robertson, 2013), which encodes the Flp recombinase to remove FRT-Pfn-kan-FRT from the genome. Bacteria were grown overnight on sMHA-hyg200, hyg-resistant

803 transformants were passaged three times on sMHA, then transformants were replica plated onto
804 sMHA-hyg200 and sMHA-kan10 to confirm sensitivity to both antibiotics (kan-cured
805 Δ*FTL1678*). pFNLTP6-gro-*FTL1678*-6×His was transformed into kan-cured Δ*FTL1678* by
806 electroporation, transformants were selected on sMHA-kan10, and FTL1678 expression was
807 confirmed by immunoblot analysis (referred to hereafter as Δ*FTL1678 trans*-complement).
808
809 *C. jejuni pgp2 complementation in trans*
810 Complementation of *C. jejuni pgp2* (CJJ81176_0915) into Δ*FTL1678* was performed as
811 described above, with several modifications. The *pgp2* gene, with the FTL1678 signal sequence
812 (amino acid residues 1-29) in place of the native Pgp2 signal sequence (amino acid residues 1-
813 18), was synthesized and inserted in pQE-60 by GenScript USA. pQE-60-*pgp2* was transformed
814 into NEB10-β *E. coli* and selection was performed on LB-amp. Pgp2-6×His was amplified from
815 pQE-60 using primers 5'FTL1678_pFNLTP6 and 3'FTL1678_pFNLTP6 (Table S8), the
816 amplicon was ligated into similarly digested pFNLTP6, pFNLTP6-gro-*pgp2*-6×His was
817 transformed into NEB10-β *E. coli*, and transformants were selected on LB-kan. Plasmids were
818 purified from kan-resistant transformants, sequence verified, then electroporated into kan-cured
819 Δ*FTL1678*. Pgp2 expression was confirmed by immunoblot analysis.
820
821 *Mouse infections*
822 All animal studies were approved by the University of Toledo Institutional Animal Care and Use
823 Committee (IACUC). Mouse infections were performed as previously described (Huntley,
824 2008), with some modifications. Briefly, *F. tularensis* strains were grown on sMHA overnight,
825 transferred to BHI agar for an additional 20-24 h, suspended in sterile PBS, and diluted to the

826 desired concentration (20 to 10^9 CFU/20 µl) based on previous OD_{600} measurements and
827 bacterial enumeration studies. Groups of 4-8 female C3H/HeN mice (6-8 weeks old; Charles
828 River Laboratories) were anesthetized with a ketamine-xylazine sedative and intranasally (i.n.)
829 infected with 20 µl of prepared bacterial suspensions. Bacterial inocula were serially-diluted and
830 plated in quadruplet on sMHA to confirm CFUs. For survival studies, mice were monitored
831 daily, for signs of disease, with health status scores (scale of 1-5, with 1 indicating healthy and 5
832 indicating mouse found dead) being recorded for each mouse. Moribund mice were humanely
833 euthanized to minimize suffering. To quantitate bacterial tissue burdens, groups of 4 mice were
834 euthanized on days 2 and 5 post-infection, blood was collected by cardiac puncture and plated
835 onto sMHA, lungs, livers, and spleens were aseptically harvested, homogenized, 25 µl of
836 PBS/mg of tissue was added to each tissue, serially-diluted, and dilutions were plated onto
837 sMHA. Following 72 h of incubation, the number of colonies per plate were counted and
838 CFU/mg (tissues) or CFU/ml (blood) were calculated based on tissue weight and dilution factor.
839 For immunization and challenge studies, groups of 4-10 mice were i.n. immunized with either
840 100-300 CFU LVS or 10^4-10^9 CFU ΔFTL1678, boosted 3-4 weeks later with either 10^3 CFU
841 LVS or 10^9 CFU ΔFTL1678, transported to the ABSL3 facility 3-weeks later, and i.n. challenged
842 with 20-120 CFU of *F. tularensis* SchuS4. Mice were monitored daily for signs of disease with
843 health status scores being recorded for each mouse.
844
845 *Membrane integrity testing*
846 Sensitivity of LVS, Δ*FTL1678*, FTL1678 *trans*-complement, and the Pgp2 *trans*-complement to
847 various antibiotics, detergents, dyes, and cell wall stressors was determined by disk diffusion
848 assays or in liquid cultures, as previously described (Wu, 2016), with some modifications.

Bacterial strains were grown on either sMHA or sMHA-kan10 (Δ*FTL1678* and complemented strains), scraped and resuspended in sterile PBS, adjusted to an OD_{600} of 0.2 (approx. 9×10^7 CFU/ml), diluted 1:1 in PBS, and 100 µl was plated onto sMHA plates using cotton tipped applicators (Puritan). Sterile paper disks (Whatman; 0.8 mm thick, 6.5 mm in diameter) were placed in the center of each plate and antibiotics, detergents, or dyes were added to the disks at the concentrations listed in Table 2. Antibiotics tested were: gentamicin (Gibco), tetracycline (Fisher Scientific), chloramphenicol (Acros Organics), ciprofloxacin (Oxoid), ampicillin (Fisher Scientific), vancomycin (Acros Organics), bacitracin (Oxoid), bacitracin (Oxoid), ciprofloxacin (Oxoid), and polymyxin B (MP Biomedicals). Detergents tested were: sodium dodecyl sulfate (SDS; anionic; Fisher Scientific), Triton X-100 (nonionic; Acros Organics), cetyltrimethyl ammonium bromide (CTAB; cationic; MP Biomedicals), 3-cholamidopropyl dimethylammonio 1-propanesulfonate (CHAPS; zwitterionic; Thermo Scientific). In addition, sensitivity to ethidium bromide (Thermo Scientific) and lysozyme (Thermo Fisher) also was tested. After 48 h, diameters of zones of inhibition around the disks were measured, with experiments performed in triplicate to confirm reproducibility. Zones of inhibition were averaged, standard deviations calculated, and all data rounded to the nearest whole number. For liquid cultures, bacteria were suspended in sMHB, adjusted to OD_{600} 0.4, and 5 ml of each bacterial suspensions was inoculated into 100 ml of either sMHB or sMHB with 5 mM hydrogen peroxide (H_2O_2), 5% sodium chloride (NaCl), or pH 5.5 (pH of sMHB is 6.5). Cultures were grown in triplicate at 37˚C with rotation at 180 rpm for 24 h with OD_{600} readings recorded every 4 h.

Electron microscopy

Electron microscopy was used to visualize differences in bacterial envelope structure and cell shape, as previously described (Wu, 2016), with some modifications. WT LVS, Δ*FTL1678*, *FTL1678 trans*-complement (FTL1678 compl), and the Pgp2 *trans*-complement (Pgp2 compl) were grown overnight in sMHB, approx. 1×10^9 CFU of each bacterial strain was pelleted by centrifugation at 7000 × *g* at 4˚C, washed three times in PBS, fixed in 3% (vol/vol) glutaraldehyde (Electron Microscopy Sciences [EMS]) for approx. 24 h, washed twice in sodium cacodylate buffer (pH 7.4; EMS) for 10 min, suspended in 1% (wt/vol) osmium tetroxide (EMS) in s-collidine buffer (pH 7.4; EMS) for 45 min at room temperature (r/t) to stain and fix the samples, washed two times with sodium cacodylate buffer for 10 min each, and tertiary fixation was performed using an aqueous saturated solution of uranyl acetate (pH 3.3; EMS) for 45 min at r/t. Samples were then dehydrated at room temperature using a series of ethanol washes: two washes with 30% ethanol for 10 min each; two washes with 50% ethanol for 10 min each; two washes with 95% ethanol for 10 min each; two washes with 100% ethanol for 10 min each; and two washes with 100% acetone for 10 min each. Samples were then infiltrated with 50% acetone and 50% embedding media (Hard Plus Resin 812, EMS) for 8 h to overnight at r/t. Samples were embedded in 100% embedding media (EMS) and allowed to polymerize for 8 h to overnight at 85°C, then sectioned at 85-90 nm, and visualized using a Tecnai G2 Spirit transmission electron microscope (FEI) at 80 kV and Radius 1.3 (Olympus) imaging software at the University of Toledo Electron Microscopy Facility. For outer membrane (OM) thickness measurements, individual bacterial cells were analyzed at 120,000×, multiple measurements (3 to 7 per bacteria) of OM thickness per bacterium were calculated by Radius 1.3 imaging software using default settings, and average OM thickness per bacterial cell were recorded (WT n=50 bacterial cells; Δ*FTL1678* n=50 bacterial cells; FTL1678 compl n=44 bacterial cells; Pgp2

compl n=33 bacterial cells). For bacterial cell width measurements, individual bacterium were analyzed at 120,000×, cell length and width were calculated using default settings, and the smallest measurement (width) per bacterium was recorded (Figure 3: WT n=175 bacterial cells, Δ*FTL1678* n=175 bacterial cells; Figure S7: WT n=119 bacterial cells; Δ*FTL1678* n=120 bacterial cells; FTL1678 compl n=119 bacterial cells; Pgp2 compl n=119 bacterial cells). Experiments were performed twice to confirm reproducibility, with two bacterial preparations fixed, stained, embedded, sectioned, and visualized per experiment.

Spheroplasting and sucrose density gradient centrifugation

Spheroplasting, osmotic lysis, and sucrose density gradient centrifugation was performed as previously described (Huntley, 2007) to determine subcellular localization of FTL1678. Briefly, the histidine-tagged FTL1678 *trans*-complement was grown in sMHB to an OD_{600} of 0.3-0.4, pelleted at 7500 × *g* for 30 min at 10˚C, supernatants were removed, pellets were resuspended in 0.75 M sucrose (in 5 mM Tris, pH 7.5) with gentle mixing, 10 mM EDTA (in 5 mM Tris, pH 7.8) was slowly added over 10 min, and the suspension was incubated for 30 min at r/t. After incubation, lysozyme was slowly added to a final concentration of 200 μg ml^{-1}, incubated for 30 min at r/t, bacteria were osmotically lysed by dilution into 4.5× volumes of molecular-grade water (Corning) over 11 min with gentle mixing, and incubated for 30 min at r/t. Lysates were centrifuged at 7,500 × *g* for 30 min at 10°C to remove intact cells and cellular debris. Supernatants were collected and centrifuged at 182,500 × *g* for 2 h at 4°C in a F37L 8 × 100 Fiberlite Ultracentrifuge rotor. Following centrifugation, supernatants were removed, membrane pellets were gently resuspended in 6 ml of resuspension buffer (25% [wt/wt] sucrose, 5 mM Tris, 30 mM $MgCl_2$, 1 tablet of Pierce Protease Inhibitor Mini Tablets, EDTA-Free [Thermo

Scientific], 5 U Benzonase [Novagen]), suspensions were incubated with gentle mixing for 30 min at room temperature to degrade DNA, and a DC protein assay (Bio-Rad) was performed to determine total protein yield. Linear sucrose gradients were prepared by layering 1.8 ml each of sucrose solutions (wt/wt; prepared in 5 mM EDTA, pH 7.5) into 14- by 95-mm ultracentrifuge tubes (Beckman) in the following order: 55%, 50%, 45%, 40%, 35%, and 30%. Membrane suspensions were layered on top of each sucrose gradient, with less than 1.5 mg of protein per gradient. Sucrose gradients were centrifuged in an SW40 swinging bucket rotor (Beckman) at 256,000 × *g* for 17 h at 4°C. After centrifugation, 500-µl fractions were collected from each gradient by puncturing the bottom of each tube and allowing fractions to drip into microcentrifuge tubes. The refractive index of each fraction was determined using a refractometer (Fisher Scientific) and correlated with a specific density in g ml^{-1} (Price, 1982) to identify outer membrane (OM; 1.17-1.20 g ml^{-1}) and inner membrane (IM; 1.13-1.14 g ml^{-1}) fractions. Sucrose gradient fractions were examined by immunoblotting as described below.

Immunoblotting

Whole cell lysates of FTL1678 *trans*-complement were prepared by suspending bacteria (pelleted at 7000 × *g*) in molecular biology grade water, diluting with SDS-PAGE loading buffer, and boiling for 10 min. Whole cell lysates, OM fractions, IM fractions, and molecular mass standards (Precision Plus protein all blue prestained protein standards; BioRad Laboratories) were separated on a 12.5% polyacrylamide gel, transferred to nitrocellulose, and blots were incubated overnight in blot block (0.1% (vol/vol) Tween 20 and 2% (wt/vol) bovine serum albumin in PBS) at 4°C. Immunoblotting was performed using rat polyclonal antiserum specific

for either *F. tularensis* OM protein FopA, *F. tularensis* IM protein SecY (Huntley, 2007) or the Penta-His HRP conjugate antibody (Qiagen).

Infections of mouse bone marrow derived macrophages (mBMDMs) and J774A.1 cells

Macrophage culture (37˚C with 5% CO_2 unless otherwise indicated) and infections were performed as previously described (Wu, 2016), with some modifications. Bone marrow macrophages were harvested from female C3H/HeN mice. Mice were euthanized by CO_2 asphyxiation and cervical dislocation. Femurs and tibias of both hind legs were aseptically-harvested, marrow was flushed from each bone with RPMI-1640 (Hyclone) containing 10% heat-inactivated fetal bovine serum ([HI-FBS], Atlanta Biologicals) and 30% supernatants from day 7 L929 cultures (ATCC). Bone marrow was disrupted by repeated passage through a 23-gauge needle and cultured for 4 days. Next, cell media was removed and replaced with RPMI containing 10% HI-FBS and 30% supernatant from day 14 L929 cultures, and cells were cultured for 2 days. Approx. 24 h before infection, media was removed, cells were harvested by scraping and centrifugation at 400 × *g* for 10 min at 10˚C, cells were enumerated using a hemocytometer, and diluted to $1x10^5$ cells in RPMI containing 10% HI-FBS. J774A.1 cells (ATCC) were cultured in Dulbecco's Modified Eagle Medium ([DMEM], Gibco) containing 10% HI-FBS. Approx. 24 h before infection, cells were harvested as described above, seeded into individual wells of 24-well plates (Corning) at a concentration of $1x10^5$ cells/well, and incubated overnight. mBMDMs and J774A.1 cells were infected with a multiplicity of infection (MOI) of 100 bacteria to 1 cell (100:1). Following infection, cells were centrifuged at 1,000 × *g* for 10 min at 4˚C, incubated at 37˚C with 5% CO_2 for 1 h, washed 1× with RPMI (or DMEM), media containing 100 µg ml^{-1} gentamicin was added to kill extracellular bacteria, cells were

incubated at 37˚C with 5% CO_2 for 1 h, washed 1× with RPMI (or DMEM), lysed with 1% saponin for 4 min, serially diluted in PBS, plated onto sMHA plates, and bacteria were enumerated (entry) after 48 h. Alternatively, after gentamicin treatment and washing, RPMI (or DMEM) containing 10% HI-FBS was added to cells and they were incubated for 6 or 24 h, lysed, serially-diluted, and plated to determine bacterial numbers.

Statistics

GraphPad Prism6 was used in various statistical analyses, including: differences in antibiotic, detergent, dye, or lysozyme susceptibility were calculated by one-way ANOVA with multiple comparisons and the Holm-Sidak post-hoc test; differences in EM measurements were determined by unpaired t-tests; differences in median time-to-death and percent survival following *F. tularensis* infection of mice were calculated using the log-rank Mantel-Cox test; differences in pathology scores of *F. tularensis*-infected tissues were calculated by two-way ANOVA with multiple comparisons and a Tukey post-hoc test. Differences in lung, liver, spleen, and blood bacterial burdens from infected mice were calculated by one-way ANOVA with multiple comparisons using R software.

Acknowledgments

We would like to acknowledge Drs. Joe Dillard and Ryan Schaub (University of Wisconsin-Madison) for all their help and expertise with peptidoglycan isolation/purification. We would also like to thank Dr. Erin Gaynor for her generous contribution of *C. jejuni* Pgp2-pGEM

plasmid construct. This work was supported by grant R01 AI093351 from the National Institute of Allergy and Infectious Disease of the National Institutes of Health (NIAID-NIH) to J.F.H.

Data Availability Statement

Data that support the findings of this study are available in the supplementary material of this article.

References

Blanot, D., Kretsovali A, Abo-Ghalia M, Mengin-Lecreulx D, van Heijenoort J, (1983) Synthesis of analogues of precursors of bacterial peptidoglycan. In: Peptides. B.a.P. Malon (ed). Berlin, Germany: Walter de Gruyter, pp. 311-314.

Bouveret, E., Benedetti H, Rigal A, Loret E, Lazdunski C (1999) In vitro characterization of peptidoglycan-associated lipoprotein (PAL)-peptidoglycan and PAL-TolB interactions. *J Bacteriol* **181**: 6306-6311.

Braun, V. (1975) Covalent lipoprotein from the outer membrane of *Escherichia coli*. *Biochim Biophys Acta* **415**: 335-377.

Braun, V., and Hantke, K. (2019) Lipoproteins: Structure, Function, Biosynthesis. *Subcell Biochem* **92**: 39-77.

1007 Braun, V., Rehn K (1969) Chemical characterization, spatial distribution and function of a
1008 lipoprotein (murein-lipoprotein) of the *E. coli* cell wall. The specific effect of trypsin on the
1009 membrane structure. *Eur J Biochem* **10**: 426-438.
1010 Braun, V., and Rehn, K. (1969) Chemical characterization, spatial distribution and function of a
1011 lipoprotein (murein-lipoprotein) of the *E. coli* cell wall. The specific effect of trypsin on the
1012 membrane structure. *Eur J Biochem* **10**: 426-438.
1013 Chaput, C., Ecobichon C, Pouradier N, Rousselle JC, Namane A, Boneca IG (2016) Role of the
1014 N-Acetylmuramoyl-l-Alanyl Amidase, AmiA, of *Helicobacter pylori* in Peptidoglycan
1015 Metabolism, Daughter Cell Separation, and Virulence. *Microb Drug Resist* **22**: 477-486.
1016 Clavel, T., Germon P, Vianney A, Portalier R, Lazzaroni JC (1998) TolB protein of *Escherichia*
1017 *coli* K-12 interacts with the outer membrane peptidoglycan-associated proteins Pal, Lpp
1018 and OmpA. *Mol Microbiol* **29**: 359-367.
1019 Das, D., Herve M, Elsliger MA, Kadam RU, Grant JC, Chiu HJ, Knuth MW, Klock HE, Miller
1020 MD, Godzik A, Lesley SA, Deacon AM, Mengin-Lecreulx D, Wilson IA (2013) Structure
1021 and function of a novel LD-carboxypeptidase a involved in peptidoglycan recycling. *J*
1022 *Bacteriol* **195**: 5555-5566.
1023 De Pascalis, R., Hahn A, Brook HM, Ryden P, Donart N, Mittereder L, Frey B, Wu TH, Elkins
1024 KL (2018) A panel of correlates predicts vaccine-induced protection of rats against
1025 respiratory challenge with virulent *Francisella tularensis*. *PLoS One* **13**: e0198140.
1026 de Pedro, M., Cava F (2015) Structural constraints and dynamics of bacterial cell wall
1027 architecture. *Front Microbiol* **6**: 449.
1028 den Blaauwen, T., de Pedro MA, Nguyen-Disteche M, Ayala JA (2008) Morphogenesis of rod-
1029 shaped sacculi. *FEMS Microbiol Rev* **32**: 321-344.

1030 Dennis, D., Inglesby TV, Henderson DA, Bartlett JG, Ascher MS, Eitzen E, Fine AD,
1031 Friedlander AM, Hauer J, Layton M, Lillibridge SR, McDade JE, Osterholm MT, O'Toole
1032 T, Parker G, Perl TM, Russell PK, and Tonat K (2001) Tularemia as a biological weapon:
1033 medical and public health management. *JAMA* **285**: 2763-2773.
1034 Denome, S., Elf PK, Henderson TA, Nelson DE, Young KD (1999) *Escherichia coli* mutants
1035 lacking all possible combinations of eight penicillin binding proteins: viability,
1036 characteristics, and implications for peptidoglycan synthesis. *J Bacteriol* **181**: 3981-3993.
1037 Dhar, S., Kumari H, Balasubramanian D, Mathee K. (2018) Cell-wall recycling and synthesis in
1038 *Escherichia coli* and *Pseudomonas aeruginosa* - their role in the development of resistance.
1039 *J Med Microbiol* **67**: 1-21.
1040 Ellis, J., Oyston PC, Green M, Titball RW (2002) Tularemia. *Clin Microbiol Rev* **15**: 631-646.
1041 Frirdich, E., Biboy J, Adams C, Lee J, Ellermeier J, Gielda LD, Dirita VJ, Girardin SE, Vollmer
1042 W, Gaynor EC (2012) Peptidoglycan-modifying enzyme Pgp1 is required for helical cell
1043 shape and pathogenicity traits in *Campylobacter jejuni*. *PLoS Pathog* **8**: e1002602.
1044 Frirdich, E., Vermeulen J, Biboy J, Soares F, Taveirne ME, Johnson JG, DiRita VJ, Girardin SE,
1045 Vollmer W, Gaynor EC (2014) Peptidoglycan LD-carboxypeptidase Pgp2 influences
1046 *Campylobacter jejuni* helical cell shape and pathogenic properties and provides the
1047 substrate for the DL-carboxypeptidase Pgp1. *J Biol Chem* **289**: 8007-8018.
1048 Gallagher, L., McKevitt M, Ramage ER, Manoil C (2008) Genetic dissection of the *Francisella*
1049 *novicida* restriction barrier. *J Bacteriol* **190**: 7830-7837.
1050 Glauner, B., Holtje JV, Schwarz U (1988) The composition of the murein of *Escherichia coli*. *J*
1051 *Biol Chem* **263**: 10088-10095.

1052 Guinane, C., Cotter PD, Ross RP, Hill C (2006) Contribution of penicillin-binding protein
1053 homologs to antibiotic resistance, cell morphology, and virulence of *Listeria*
1054 *monocytogenes* EGDe. *Antimicrob Agents Chemother* **50**: 2824-2828.
1055 Hall, J., Woolard MD, Gunn BM, Craven RR, Taft-Benz S, Frelinger JA, Kawula TH (2008)
1056 Infected-host-cell repertoire and cellular response in the lung following inhalation of
1057 *Francisella tularensis* Schu S4, LVS, or U112. *Infect Immun* **76**: 5843-5852.
1058 Heidrich, C., Templin MF, Ursinus A, Merdanovic M, Berger J, Schwarz H, de Pedro MA,
1059 Holtje JV (2001) Involvement of N-acetylmuramyl-L-alanine amidases in cell separation
1060 and antibiotic-induced autolysis of *Escherichia coli*. *Mol Microbiol* **41**: 167-178.
1061 Heidrich, C., Ursinus A, Berger J, Schwarz H, Holtje JV (2002) Effects of multiple deletions of
1062 murein hydrolases on viability, septum cleavage, and sensitivity to large toxic molecules in
1063 *Escherichia coli*. *J Bacteriol* **184**: 6093-6099.
1064 Herve, M., Boniface A, Gobec S, Blanot D, Mengin-Lecreulx D (2007) Biochemical
1065 characterization and physiological properties of *Escherichia coli* UDP-N-
1066 acetylmuramate:L-alanyl-gamma-D-glutamyl-meso-diaminopimelate ligase. *J Bacteriol*
1067 **189**: 3987-3995.
1068 Holtje, J. (1998) Growth of the stress-bearing and shape-maintaining murein sacculus of
1069 *Escherichia coli*. *Microbiol Mol Biol Rev* **62**: 181-203.
1070 Huntley, J., Conley PG, Hagman KE, Norgard MV (2007) Characterization of *Francisella*
1071 *tularensis* outer membrane proteins. *J Bacteriol* **189**: 561-574.
1072 Huntley, J., Conley PG, Rasko DA, Hagman KE, Apicella MA, Norgard MV (2008) Native
1073 outer membrane proteins protect mice against pulmonary challenge with virulent type A
1074 *Francisella tularensis*. *Infect Immun* **76**: 3664-3671.

1075 Jenkins, C., Wallis R, Allcock N, Barnes KB, Richards MI, Auty JM, Galyov EE, Harding SV,
1076 Mukamolova GV (2019) The lytic transglycosylase, LtgG, controls cell morphology and
1077 virulence in *Burkholderia pseudomallei*. *Sci Rep* **9**: 11060.
1078 Johnson, J., Fisher JF, Mobashery S (2013) Bacterial cell-wall recycling. *Ann N Y Acad Sci*
1079 **1277**: 54-75.
1080 Jones, C., Napier BA, Sampson TR, Llewellyn AC, Schroeder MR, Weiss DS (2012) Subversion
1081 of host recognition and defense systems by *Francisella* spp. *Microbiol Mol Biol Rev* **76**:
1082 383-404.
1083 Juan, C., Torrens G, Barcelo IM, Oliver A (2018) Interplay between Peptidoglycan Biology and
1084 Virulence in Gram-Negative Pathogens. *Microbiol Mol Biol Rev* **82**: e00033-00018.
1085 Keim, P., Johansson A, Wagner DM (2007) Molecular epidemiology, evolution, and ecology of
1086 *Francisella*. *Ann N Y Acad Sci* **1105**: 30-66.
1087 Kijek, T., Mou S, Bachert BA, Kuehl KA, Williams JA, Daye SP, Worsham PL, Bozue JA
1088 (2019) The D-alanyl-d-alanine carboxypeptidase enzyme is essential for virulence in the
1089 Schu S4 strain of *Francisella tularensis* and a dacD mutant is able to provide protection
1090 against a pneumonic challenge. *Microb Pathog* **137**: 103742.
1091 Kingry, L., Petersen JM (2014) Comparative review of *Francisella tularensis* and *Francisella*
1092 *novicida*. *Front Cell Infect Microbiol* **4**: 35.
1093 Knodler, L.A., Vallance, B.A., Hensel, M., Jackel, D., Finlay, B.B., and Steele-Mortimer, O.
1094 (2003) *Salmonella* type III effectors PipB and PipB2 are targeted to detergent-resistant
1095 microdomains on internal host cell membranes. *Mol Microbiol* **49**: 685-704.
1096 Korza, H., Bochtler M (2005) *Pseudomonas aeruginosa* LD-carboxypeptidase, a serine peptidase
1097 with a Ser-His-Glu triad and a nucleophilic elbow. *J Biol Chem* **280**: 40802-40812.

1098 Leduc, M., Ishidate K, Shakibai N, Rothfield L (1992) Interactions of *Escherichia coli*
1099 membrane lipoproteins with the murein sacculus. *J Bacteriol* **174**: 7982-7988.
1100 Lenz, J., Hackett KT, Dillard JP (2017) A Single Dual-Function Enzyme Controls the Production
1101 of Inflammatory NOD Agonist Peptidoglycan Fragments by *Neisseria gonorrhoeae*. *MBio*
1102 **8**: e01464-01417.
1103 Lenz, J.D., Hackett, K.T., and Dillard, J.P. (2017) A Single Dual-Function Enzyme Controls the
1104 Production of Inflammatory NOD Agonist Peptidoglycan Fragments by *Neisseria*
1105 *gonorrhoeae*. *MBio* **8**.
1106 Leulier, F., Parquet C, Pili-Floury S, Ryu JH, Caroff M, Lee WJ, Mengin-Lecreulx D, Lemaitre
1107 B (2003) The *Drosophila* immune system detects bacteria through specific peptidoglycan
1108 recognition. *Nat Immunol* **4**: 478-484.
1109 Lund, P., Tramonti, A., and De Biase, D. (2014) Coping with low pH: molecular strategies in
1110 neutralophilic bacteria. *FEMS Microbiol Rev* **38**: 1091-1125.
1111 Maier, T., Havig A, Casey M, Nano FE, Frank DW, Zahrt TC (2004) Construction and
1112 characterization of a highly efficient *Francisella* shuttle plasmid. *Appl Environ Microbiol*
1113 **70**: 7511-7519.
1114 Mengin-Lecreulx, D., and Lemaitre, B. (2005) Structure and metabolism of peptidoglycan and
1115 molecular requirements allowing its detection by the *Drosophila* innate immune system. *J*
1116 *Endotoxin Res* **11**: 105-111.
1117 Metz, R., Henning S, Hammes WP (1986a) LD-carboxypeptidase activity in *Escherichia coli*. I.
1118 The LD-carboxypeptidase activity in ether treated cells. *Arch Microbiol* **144**: 175-180.

1119 Metz, R., Henning S, Hammes WP (1986b) LD-carboxypeptidase activity in *Escherichia coli*. II.
1120 Isolation, purification and characterization of the enzyme from *E. coli* K 12. *Arch*
1121 *Microbiol* **144**: 181-186.
1122 Meyer, K., Addy C, Akashi S, Roper DI, Tame JRH (2018) The crystal structure and oligomeric
1123 form of *Escherichia coli* L,D-carboxypeptidase A. *Biochem Biophys Res Commun* **499**:
1124 594-599.
1125 Minor, P. (2015) Live attenuated vaccines: Historical successes and current challenges. *Virology*
1126 **479-480**: 379-392.
1127 Mishra, S., and Imlay, J. (2012) Why do bacteria use so many enzymes to scavenge hydrogen
1128 peroxide? *Arch Biochem Biophys* **525**: 145-160.
1129 Nelson, D., Young KD (2000) Penicillin binding protein 5 affects cell diameter, contour, and
1130 morphology of *Escherichia coli*. *J Bacteriol* **182**: 1714-1721.
1131 Park, J., Uehara T (2008) How bacteria consume their own exoskeletons (turnover and recycling
1132 of cell wall peptidoglycan). *Microbiol Mol Biol Rev* **72**: 211-227.
1133 Pazos, M., and Peters, K. (2019) Peptidoglycan. *Subcell Biochem* **92**: 127-168.
1134 Pennartz, A., Genereux C, Parquet C, Mengin-Lecreulx D, Joris B (2009) Substrate-induced
1135 inactivation of the *Escherichia coli* AmiD N-acetylmuramoyl-L-alanine amidase highlights
1136 a new strategy to inhibit this class of enzyme. *Antimicrob Agents Chemother* **53**: 2991-
1137 2997.
1138 Petrosino, J.F., Xiang, Q., Karpathy, S.E., Jiang, H., Yerrapragada, S., Liu, Y., Gioia, J.,
1139 Hemphill, L., Gonzalez, A., Raghavan, T.M., Uzman, A., Fox, G.E., Highlander, S.,
1140 Reichard, M., Morton, R.J., Clinkenbeard, K.D., and Weinstock, G.M. (2006)

1141 Chromosome rearrangement and diversification of *Francisella tularensis* revealed by the
1142 type B (OSU18) genome sequence. *J Bacteriol* **188**: 6977-6985.
1143 Price, C. (1982) Centrifugation in density gradients. *Academic Press*: 335-343.
1144 Priyadarshini, R., de Pedro MA, Young KD (2007) Role of peptidoglycan amidases in the
1145 development and morphology of the division septum in *Escherichia coli*. *J Bacteriol* **189**:
1146 5334-5347.
1147 Priyadarshini, R., Popham DL, Young KD (2006) Daughter cell separation by penicillin-binding
1148 proteins and peptidoglycan amidases in *Escherichia coli*. *J Bacteriol* **188**: 5345-5355.
1149 Qin, A., Scott DW, Thompson JA, Mann BJ (2009) Identification of an essential *Francisella*
1150 *tularensis* subsp. *tularensis* virulence factor. *Infect Immun* **77**: 152-161.
1151 Ray, K., Marteyn B, Sansonetti PJ, Tang CM (2009) Life on the inside: the intracellular lifestyle
1152 of cytosolic bacteria. *Nat Rev Microbiol* **7**: 333-340.
1153 Ren, G., Champion MM, Huntley JF (2014) Identification of disulfide bond isomerase substrates
1154 reveals bacterial virulence factors. *Mol Microbiol* **94**: 926-944.
1155 Roberts, L., Powell DA, Frelinger JA (2018) Adaptive Immunity to *Francisella tularensis* and
1156 Considerations for Vaccine Development. *Front Cell Infect Microbiol* **8**: 115.
1157 Robertson, G., Child R, Ingle C, Celli J, Norgard MV (2013) IglE is an outer membrane-
1158 associated lipoprotein essential for intracellular survival and murine virulence of type A
1159 *Francisella tularensis*. *Infect Immun* **81**: 4026-4040.
1160 Russo, T., MacDonald U, Beanan JM, Olson R, MacDonald IJ, Sauberan SL, Luke NR, Schultz
1161 LW, Umland TC (2009) Penicillin-binding protein 7/8 contributes to the survival of
1162 *Acinetobacter baumannii in vitro* and *in vivo*. *J Infect Dis* **199**: 513-521.

1163 Scheurwater, E., Reid CW, Clarke AJ (2008) Lytic transglycosylases: bacterial space-making
1164 autolysins. *Int J Biochem Cell Biol* **40**: 586-591.
1165 Silhavy, T.J., Kahne, D., and Walker, S. (2010) The bacterial cell envelope. *Cold Spring Harb*
1166 *Perspect Biol* **2**: a000414.
1167 Sjostedt, A. (2007) Tularemia: history, epidemiology, pathogen physiology, and clinical
1168 manifestations. *Ann N Y Acad Sci* **1105**: 1-29.
1169 Spidlova, P., Stojkova P, Dankova V, Senitkova I, Santic M, Pinkas D, Philimonenko V, Stulik J
1170 (2018) *Francisella tularensis* D-Ala D-Ala Carboxypeptidase DacD Is Involved in
1171 Intracellular Replication and It Is Necessary for Bacterial Cell Wall Integrity. *Front Cell*
1172 *Infect Microbiol* **8**: 111.
1173 Steiner, D., Furuya Y, Jordan MB, Metzger DW (2017) Protective Role for Macrophages in
1174 Respiratory *Francisella tularensis* Infection. *Infect Immun* **85**.
1175 Stenbak, C., Ryu JH, Leulier F, Pili-Floury S, Parquet C, Herve M, Chaput C, Boneca IG, Lee
1176 WJ, Lemaitre B, Mengin-Lecreulx D (2004) Peptidoglycan molecular requirements
1177 allowing detection by the *Drosophila* immune deficiency pathway. *J Immunol* **173**: 7339-
1178 7348.
1179 Sycuro, L., Pincus Z, Gutierrez KD, Biboy J, Stern CA, Vollmer W, Salama NR (2010)
1180 Peptidoglycan crosslinking relaxation promotes *Helicobacter pylori*'s helical shape and
1181 stomach colonization. *Cell* **141**: 822-833.
1182 Sycuro, L., Rule CS, Petersen TW, Wyckoff TJ, Sessler T, Nagarkar DB, Khalid F, Pincus Z,
1183 Biboy J, Vollmer W, Salama NR (2013) Flow cytometry-based enrichment for cell shape
1184 mutants identifies multiple genes that influence *Helicobacter pylori* morphology. *Mol*
1185 *Microbiol* **90**: 869-883.

1186 Templin, M., Ursinus A, Holtje JV (1999) A defect in cell wall recycling triggers autolysis
1187 during the stationary growth phase of *Escherichia coli*. *EMBO J* **18**: 4108-4117.
1188 Typas, A., Banzhaf M, Gross CA, Vollmer W (2011) From the regulation of peptidoglycan
1189 synthesis to bacterial growth and morphology. *Nat Rev Microbiol* **10**: 123-136.
1190 Ursinus, A., Steinhaus H, Holtje JV (1992) Purification of a nocardicin A-sensitive LD-
1191 carboxypeptidase from *Escherichia coli* by affinity chromatography. *J Bacteriol* **174**: 441-
1192 446.
1193 van Heijenoort, J. (2011) Peptidoglycan hydrolases of *Escherichia coli*. *Microbiol Mol Biol Rev*
1194 **75**: 636-663.
1195 Vollmer, W., and Bertsche, U. (2008) Murein (peptidoglycan) structure, architecture and
1196 biosynthesis in *Escherichia coli*. *Biochim Biophys Acta* **1778**: 1714-1734.
1197 Walburger, A., Lazdunski C, Corda Y (2002) The Tol/Pal system function requires an interaction
1198 between the C-terminal domain of TolA and the N-terminal domain of TolB. *Mol*
1199 *Microbiol* **44**: 695-708.
1200 Weaver, A.I., Jimenez-Ruiz, V., Tallavajhala, S.R., Ransegnola, B.P., Wong, K.Q., and Dorr, T.
1201 (2019) Lytic transglycosylases RlpA and MltC assist in *Vibrio cholerae* daughter cell
1202 separation. *Mol Microbiol* **112**: 1100-1115.
1203 Wu, X., Ren G, Gunning WT 3rd, Weaver DA, Kalinoski AL, Khuder SA, Huntley JF (2016)
1204 FmvB: A *Francisella tularensis* Magnesium-Responsive Outer Membrane Protein that
1205 Plays a Role in Virulence. *PLoS One* **11**: e0160977.
1206 Wu, X., Ren G, Huntley JF (2015) Generating Isogenic Deletions (Knockouts) in *Francisella*
1207 *tularensis*, a Highly-infectious and Fastidious Gram-negative Bacterium. *Bio Protoc* **5**:
1208 e1500.

1209

Table 1. Specific activity and substrate specificity of FTL1678 and FTT0101 enzymes

Substrate	Specific activity (nmol/min/mg of protein) [a]	
	FTL1678	FTT0101
A_2pm-containing substrates		
GlcNAc-anhydroMurNAc-L-Ala-γ-D-Glu-*meso*-A_2pm-D-Ala (TCT)	21.5 ± 1.34	29.0 ± 1.42
GlcNAc-MurNAc-L-Ala-γ-D-Glu-*meso*- A_2pm-D-Ala (PG monomer)	15.6 ± 0.79	24.2 ± 1.80
TCT dimer (4-3 D,D-crosslinkage)	7.7 ± 0.30	11.8 ± 0.53
MurNAc-L-Ala-γ-D-Glu-*meso*-A2pm-D-Ala	5.8 ± 0.66	7.8 ± 1.10
UDP-MurNAc-L-Ala-γ-D-Glu-*meso*-A_2pm-D-Ala	4.6 ± 0.52	6.3 ± 0.26
L-Ala-γ-D-Glu-*meso*-A_2pm-D-Ala (free tetrapeptide)	3.4 ± 0.59	8.0 ± 0.92
MurNAc-L-Ala-γ-D-Glu-*meso*-A_2pm-D-Ala-D-Ala (pentapeptide)	9.8 ± 1.22	6.2 ± 0.56
UDP-MurNAc-L-Ala-γ-D-Glu-*meso*-A_2pm-D-Ala-D-Ala (pentapeptide)	5.9 ± 0.14	6.4 ± 0.17
L-Lysine-containing substrates		
MurNAc-L-Ala-γ-D-Glu-L-Lys-D-Ala	1.3 ± 0.28	2.1 ± 0.36
L-Ala-γ-D-Glu-L-Lys-D-Ala	0.7 ± 0.14	2.1 ± 0.28
UDP-MurNAc-L-Ala-γ-D-Glu-L-Lys-D-Ala-D-Ala	1.2 ± 0.26	1.7 ± 0.20
Others		
GlcNAc-MurNAc-L-Ala-γ-D-Glu-*meso*-A_2pm(NH_2)-D-Ala		Very low (<0.5)
GlcNAc-MurNAc-L-Ala-γ-D-Glu(NH_2)-*meso*-A_2pm-D-Ala		Not detected [b]
GlcNAc-MurNAc-L-Ala-γ-D-Glu(NH_2)-*meso*-A_2pm(NH_2)-D-Ala		Not detected [b]
Peptidoglycan polymer		Not detected [b]

[a] Standard enzyme assay conditions are described in the Materials and Methods. Values represent the mean ± standard deviation of triplicate experiments.

[b] Not detected indicates that no formation of the corresponding disaccharide-tripeptide (HPLC) and/or release of alanine (amino acid analyzer) was detected in the assay conditions used.

Table 2. Sensitivity of WT and Δ*FTL1678* to antibiotics, detergents, and dyes

Compound	Concentration (µg/disk)	Average zone of inhibition, mm (mean ± SD)[a]	
		WT	**Δ*FTL1678***
Gentamicin	4	3 ± 0	1 ± 0 (R)
Tetracycline	5	2 ± 0	1 ± 0 (R)
Chloramphenicol	5	3 ± 0	1 ± 0 (R)
Ciprofloxacin	5	5 ± 0	2 ± 0 (R)
Ampicillin	200	3 ± 0	4 ± 0 (S)
Vancomycin	20	1 ± 0	3 ± 0 (S)
Bacitracin	182	1 ± 0	1 ± 0
Polymyxin B	100	1 ± 0	1 ± 0
Lysozyme	1000	1 ± 0	2 ± 0 (S)
Ethidium Bromide	5	3 ± 0	1 ± 0 (R)
Triton-X100	750	3 ± 0	3 ± 0
SDS	1000	1 ± 0	2 ± 0 (S)
CTAB	50	1 ± 0	1 ± 0
CHAPS	50	1 ± 0	1 ± 0

[a] (R) indicates Δ*FTL1678* is significantly more resistant than WT by one-way ANOVA ($P<0.05$)

[a] (S) indicates Δ*FTL1678* is significantly more sensitive than WT by one-way ANOVA ($P<0.05$)

Figure 1. Amino acid alignment of bacterial L,D-carboxypeptidases. Clustal Omega amino acid alignment of *E. coli* LdcA (BAA36050.1), *P. aeruginosa* LdcA (Q9HTZ1), *N. gonorrhoeae* LdcA (YP_208343.1), *F. tularensis* Type B FTL1678, and *F. tularensis* Type A FTT0101, and *C. jejuni* Pgp2 (WP_002856863). Percent identities (pid), compared to *E. coli* LdcA, are indicated. Black shading indicates similar residues. Red shading indicates the catalytic triad.

Figure 2. FTL1678 is OM-associated. Spheroplasting, osmotic lysis, and sucrose density gradient centrifugation were performed to separate inner membranes (IM) and outer membranes (OM) from *F. tularensis* Δ*FTL1678 trans*-complemented with a 6×histidine-tagged FTL1678. Whole-cell lysates (WCL), OM fractions, and IM fractions were separated by SDS-PAGE, transferred to nitrocellulose, and immunoblotting was performed using antisera specific for the OM control protein FopA (αFopA), IM control protein SecY (αSecY), or histidine-tagged FTL1678.

Figure 3. Deletion of FTL1678 alters bacterial morphology. Electron micrograph images of: (A) Wild-type LVS or (B) Δ*FTL1678* grown in sMHB to OD_{600} of 0.4. Scale bars represent 100 nm. Representative images shown; (C) Outer membrane [OM] thickness measurements [nm] were determined for WT and Δ*FTL1678*, with n=50 bacterial cells analyzed per experimental group, multiple width measurements recorded per individual bacterium, and average width/bacterium recorded; (D) Cell width measurements [nm] for WT and Δ*FTL1678*, with n=175 bacterial cells analyzed per experimental group. **** indicates $P<0.0001$.

Figure 4. Deletion of *FTL1678* affects sensitivity to envelope stress. WT and Δ*FTL1678* were grown in 100 ml sMHB: (A) at 37˚C, (B) at 40˚C, (C) addition of 60 µM $CuCl_2$, (D) addition of 5 mM H_2O_2, (E) addition of 5% NaCl, or (F) pH 5.5. Bacteria were grown in triplicate for 24 h and OD_{600} measurements were recorded every 4 h. Error bars represent standard deviation at each time point.

Figure 5. Δ*FTL1678* is fully-attenuated in a mouse pulmonary infection model. (A) Groups of 5 C3H/HeN mice were intranasally-infected with 10^5 CFU of either wild-type WT, Δ*FTL1678*, or Δ*FTL1678 trans*-complemented with *FTL1678* [FTL1678 compl]. Animal health was monitored daily through day 21 post-infection. **** indicates $P<0.0001$; (B) Lungs, livers, spleens, and blood were aseptically harvested from mice infected with 10^4 CFU of either WT or Δ*FTL1678* on days 2 and 5 post-infection and plated to enumerate bacterial numbers. * indicates $P<0.01$; (C) Groups of 5 C3H/HeN mice were intranasally-infected with 10^5 CFU of either LVS, Δ*FTL1678*, FTL1678 *trans*-complement [FTL1678 compl], or *C. jejuni* Pgp2 *trans*-complement [Pgp2 compl]. Animal health was monitored through day 21 post-infection. ** indicates $P<0.01$.

Figure 6. FTL1678 is required for *F. tularensis* replication in macrophages. (A) J774A.1 macrophages or mouse bone marrow-derived macrophages (mBMDMs) were infected with WT or Δ*FTL1678* at an MOI of 100:1 and bacterial numbers were enumerated at entry (0 h), 6 h, and 24 h post-infection. (B) Fold change in bacterial numbers from 6 to 24 h post-infection was calculated. * indicates $P< 0.01$.

Figure 7. Δ*FTL1678* protects against fully-virulent Type A *F. tularensis* SchuS4. (A) Groups of 5 C3H/HeN mice were intranasally infected with either 10^5 CFU WT or 10^5, 10^7, or 10^9 CFU Δ*FTL1678*. On day 29 post-infection, mice were boosted with 10^9 CFU Δ*FTL1678* and animal health was monitored daily through day 50 post-infection. *** $P<0.001$; (B) Mice from A were intranasally-challenged with 120 CFU of wild-type SchuS4 [BSL3; 6× LD50]. Animal health was monitored daily through day 26 post-infection. * indicates $P<0.001$.

Figure 8. Δ*FTL1678* does not induce tissue damage. (A) Hematoxylin and eosin (H&E)-stained lungs, livers, and spleens were examined from either uninfected, *F. tularensis* WT LVS-, or Δ*FTL1678*-infected mice at 10× objective. (B) Tissues were graded on a scale of 0 to 4, with 4 being the most severe. * indicates $P<0.05$.

Figure 9. Model of *F. tularensis* peptidoglycan synthesis and recycling pathways. Bioinformatic analyses were used to predict proteins that may be involved in peptidoglycan synthesis and recycling in *F. tularensis*. *F. tularensis* LVS gene locus tags are indicated, with *E. coli* or Gram-negative ortholog protein names. OM, outer membrane. IM, inner membrane. GlcNAc, *N*-acetylglucosamine. MurNAc, *N*-acetylmuramic acid. Pal, OM-localized peptidoglycan-associated lipoprotein. TolB, periplasmic protein that interacts with Pal and peptidoglycan. HMM PBP, high molecular weight penicillin binding protein. LMM PBP, low molecular weight penicillin binding protein.

1287 **Supporting Information**

1288

1289 **Table S1.** HPLC retention times of peptidoglycan (PG) compounds analyzed in this study

1290

1291 **Table S2.** Endopeptidase activity of FTL1678

1292

1293 **Table S3.** Specific activity of FTL1678, FTL1678 double mutants, and FTL1678 triple mutants

1294 to the TCT monomer

1295

1296 **Table S4.** Bioinformatic analyses of FTL1678 localization

1297

1298 **Table S5.** Sensitivity of WT LVS, Δ*FTL1678*, *FTL1678 trans*-complement, and Pgp2 *trans*-

1299 complement to antibiotics, detergents, and dyes

1300

1301 **Table S6.** Sensitivity of WT *F. tularensis* SchuS4 and Δ*FTT0101* to antibiotics, detergents, and

1302 dyes

1303

1304 **Table S7.** Bacterial strains and plasmids used in this study

1305

1306 **Table S8.** Primers used in this study

1307

1308

Figure S1. FTL1678 contains a putative L,D-carboxypeptidase domain. NCBI Conserved Domain search results for *F. tularensis* FTL1678.

Figure S2. Activity of FTL1678 and controls on GlcNAc-anhydroMurNAc-tetrapeptide (TCT). (A) Structure of TCT with the LdcA cleavage site indicated (blue arrow). (B) HPLC analysis of reaction mixtures obtained following incubation of TCT in the presence of either FTL1678, vector control extract, or buffer alone. The enzymatic assay and HPLC conditions used are outlined in Materials and Methods.

Figure S3. Activity of FTL1678 and controls on the free tetrapeptide, L-Ala-γ-D-Glu-*meso*-A_2pm-D-Ala. HPLC analysis of reaction mixtures obtained following incubation of L-Ala-γ-D-Glu-*meso*-A_2pm-D-Ala (Tetra) in the presence of buffer alone, extract from the vector control, or purified FTL1678. A peak of L-Ala-γ-D-Glu-*meso*-A_2pm product (Tri) was only detected in the presence of FTL1678. FTL1678 enzyme activity was not affected by the presence of either 2.5 mM $MgCl_2$ or 5 mM EDTA added to the reaction mixtures. The enzymatic assay and HPLC conditions used are outlined in Materials and Methods.

Figure S4. *F. tularensis* TolB is OM-localized. Spheroplasting, osmotic lysis, and sucrose density gradient centrifugation were performed to separate inner membranes (IM) and outer membranes (OM) from *F. tularensis* Δ*FTL1678 trans*-complemented with a 6×histidine-tagged FTL1678. Whole-cell lysates (WCL), OM fractions, and IM fractions were separated by SDS-PAGE, transferred to nitrocellulose, and immunoblotting was performed using antisera specific for the periplasmic protein TolB (αTolB).

Figure S5. Δ*FTL1678* does not have a growth defect. WT and Δ*FTL1678* were grown in sMHB for 24 h at 37˚C. Samples were taken every 4 h for (A) OD_{600} measurements and (B) CFU enumeration following serial-dilution and plating.

Figure S6. Δ*FTL1678* has septation defects. Transmission electron micrograph images of Δ*FTL1678* bacteria showing aberrant septal formation and reduced ability to separate cells. Images taken at: (A) 49,000×, scale bar represents 200 nm; and (B) 6,800×, scale bar represents 2 µm. In (A), red arrows point to formed septa that have not separated in Δ*FTL1678* bacteria and white arrows point to new septa that are forming in Δ*FTL1678* bacteria. Experiments were performed twice to confirm reproducibility, with two bacterial preparations fixed, stained, embedded, sectioned, and visualized per experiment. Representative images shown.

Figure S7. *FTL1678 trans*-complement and *C. jejuni* Pgp2 *trans*-complement restore *F. tularensis* phenotype. Transmission electron micrograph images of: (A) Δ*FTL1678 trans*-complemented with *FTL1678* [FTL1678 compl] or (B) Δ*FTL1678 trans*-complemented with *C. jejuni pgp2* [Pgp2 compl]. Bacteria were grown in sMHB to OD_{600} of 0.4. Scale bars represent 100 nm. (C) Outer membrane thickness [WT n=50; Δ*FTL1678* n=50; FTL1678 compl n=44; Pgp2 compl n=33] and (D) cell width [WT n=119; Δ*FTL1678* n=120; FTL1678 compl n=119; Pgp2 compl n=119] of FTL1678 compl and Pgp2 compl were compared to WT LVS and Δ*FTL1678*. **** indicates $P<0.0001$.

Figure S8. *FTL1678 trans*-complement and *C. jejuni* Pgp2 *trans*-complement exhibit similar phenotypes to stressors as WT *F. tularensis*. WT LVS [WT], Δ*FTL1678*, Δ*FTL1678* *trans*-complemented with *FTL1678* [FTL1678 compl], or Δ*FTL1678* *trans*-complemented with *C. jejuni pgp2* [Pgp2 compl] were grown in either: (A) sMHB; (B) sMHB with 5 mM H_2O_2; (C) sMHB with 5% NaCl; or (D) sMHB at pH 5.5. Cultures were incubated for 24 h and OD_{600} measurements were recorded every 4 h.

Figure S9. FTT0101 is not required for *F. tularensis* Type A strain SchuS4 virulence. C3H/HeN mice were intranasally infected with either 80 CFU SchuS4 (n=3 mice) or 12 CFU Δ*FTT0101* (n=5 mice).

Figure S10. Individual amino acids of the LdcA catalytic triad are not essential for *F. tularensis* virulence. Groups of 5 C3H/HeN mice were intranasally-infected with 10^5 CFU of either *F. tularensis* WT LVS, Δ*FTL1678*, Δ*FTL1678* *trans*-complemented with FTL1678 (FTL1678 compl), Δ*FTL1678* *trans*-complemented with S134A (S134A), Δ*FTL1678* *trans*-complemented with E239A (E239A), or Δ*FTL1678* *trans*-complemented with H308A (H308A). Animal health was monitored daily through day 21 post-infection. ** $P<0.01$.

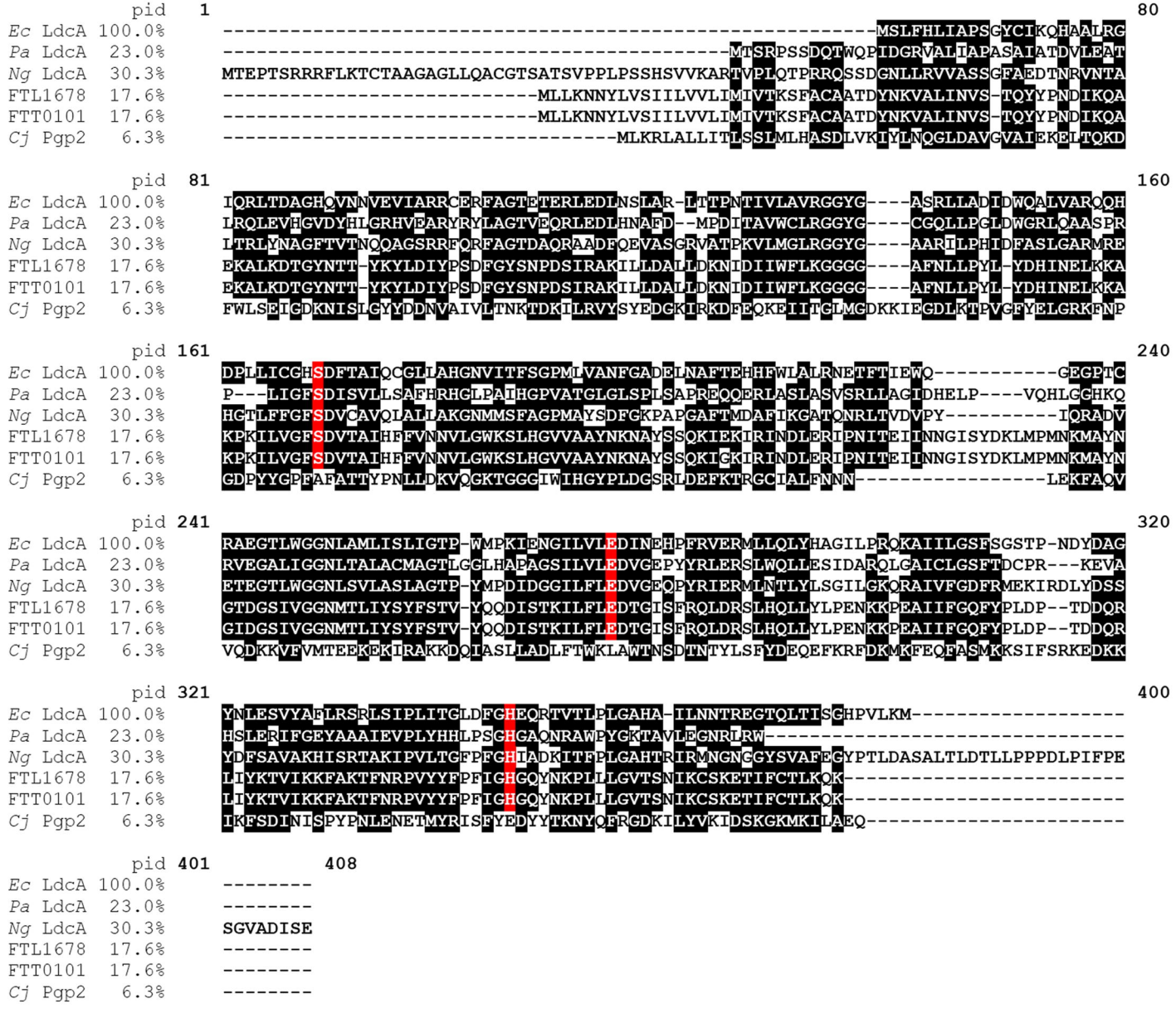
pid 1 80
Ec LdcA 100.0%
Pa LdcA 23.0%
Ng LdcA 30.3%
FTL1678 17.6%
FTT0101 17.6%
Cj Pgp2 6.3%
pid 81 160
pid 161 240
pid 241 320
pid 321 400
pid 401 408
SGVADISE

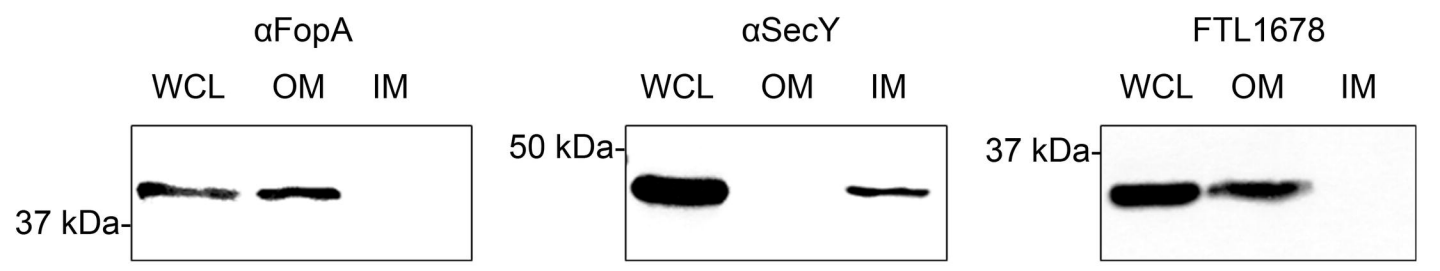
αFopA
WCL
OM
IM
37 kDa
αSecY
WCL
OM
IM
50 kDa
FTL1678
WCL
OM
IM
37 kDa

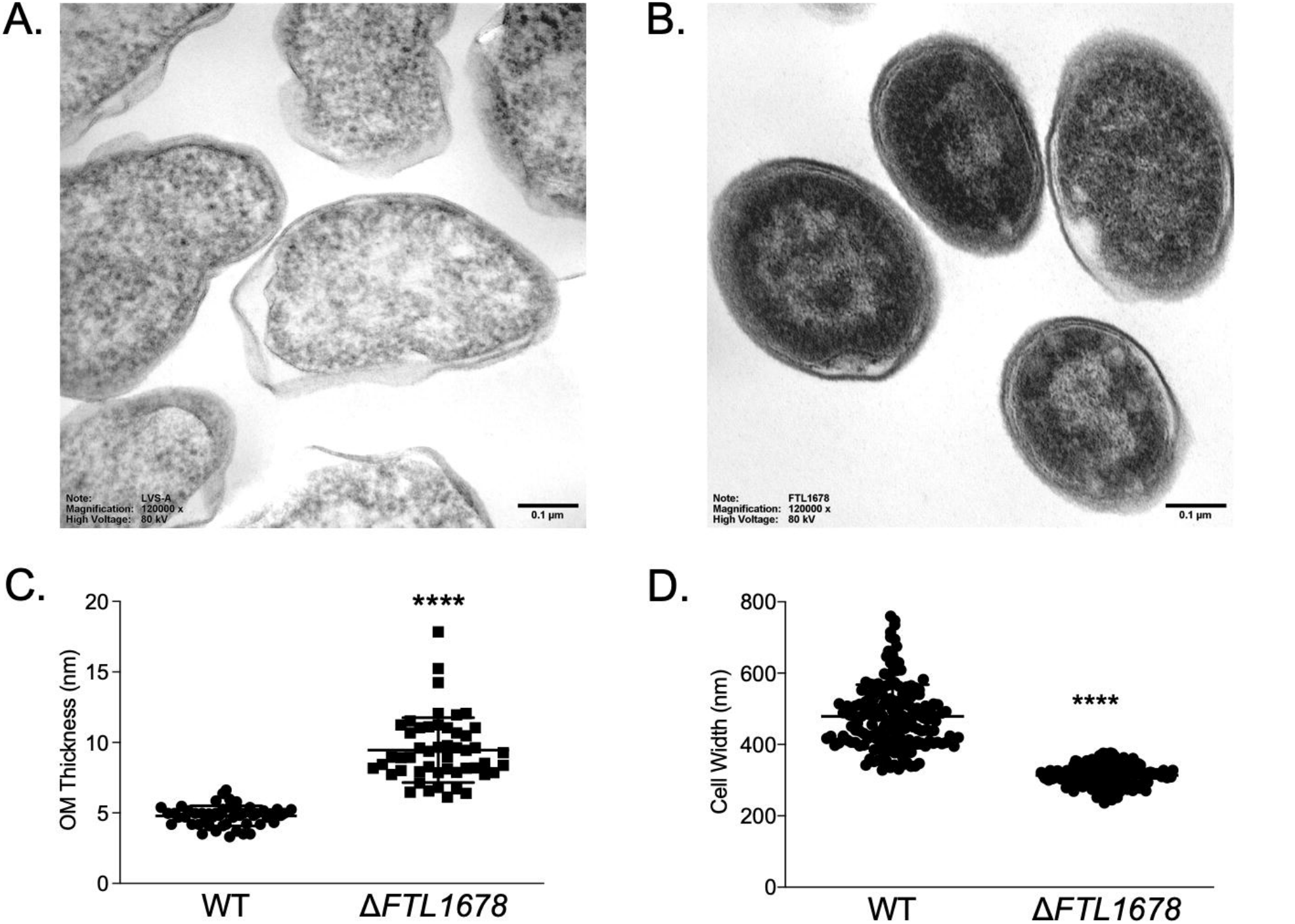
A.
Note: LVS-A
Magnification: 120000 x
High Voltage: 80 kV
0.1 µm
B.
Note: FTL1678
Magnification: 120000 x
High Voltage: 80 kV
0.1 µm
C.
OM Thickness (nm)
20
15
10
5
0
****
WT
ΔFTL1678
D.
Cell Width (nm)
800
600
400
200
0
****
WT
ΔFTL1678

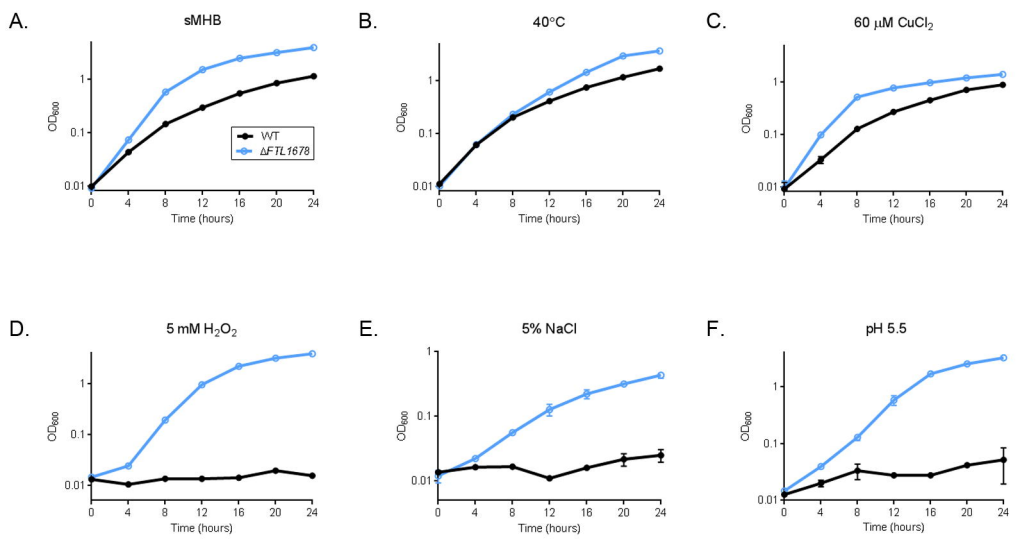
A.
sMHB
B.
40°C
C.
60 μM CuCl2
D.
5 mM H2O2
E.
5% NaCl
F.
pH 5.5
OD600
Time (hours)
WT
ΔFTL1678

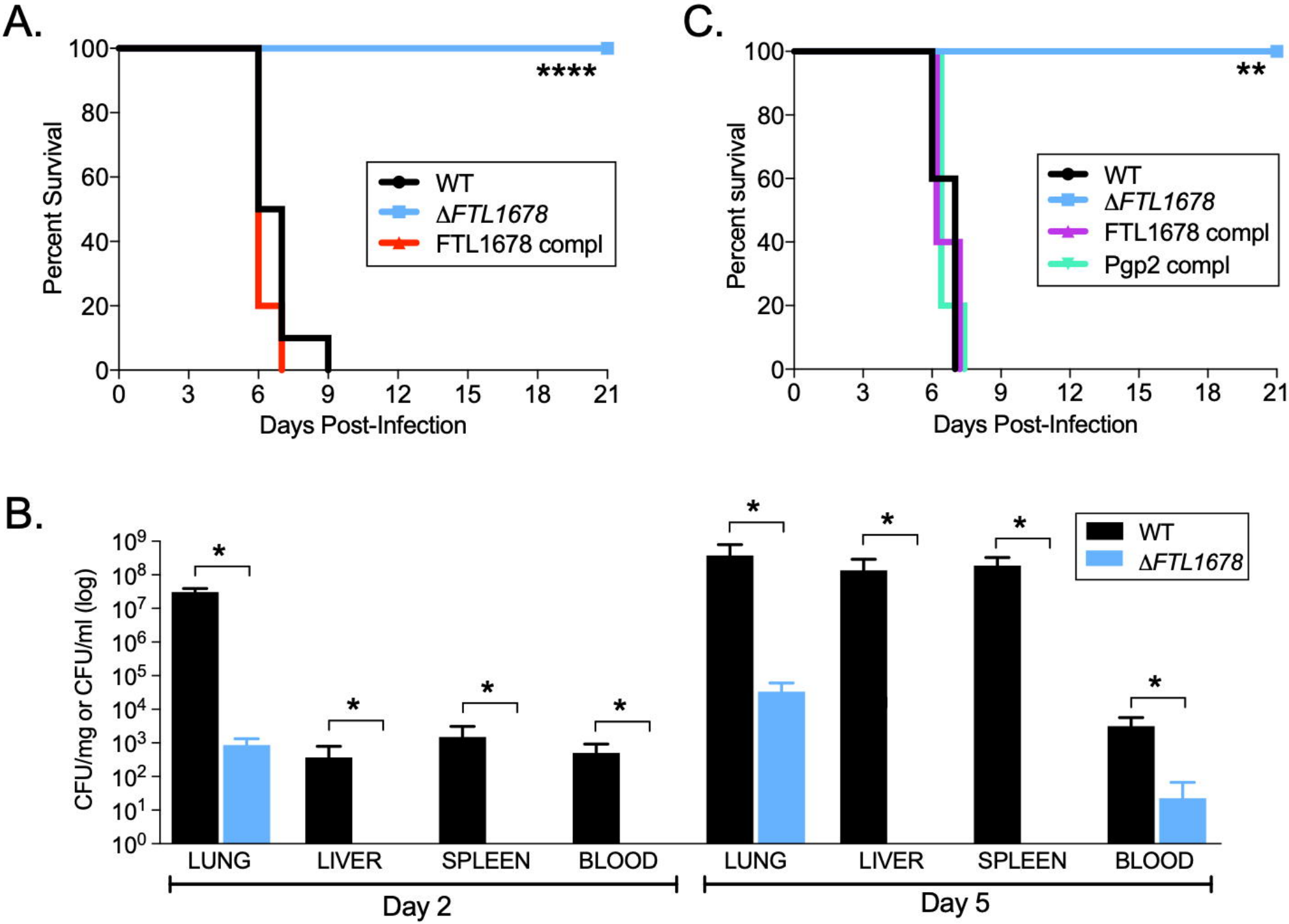
A.
Percent Survival
Days Post-Infection
WT
ΔFTL1678
FTL1678 compl
****
C.
Percent survival
Days Post-Infection
WT
ΔFTL1678
FTL1678 compl
Pgp2 compl
**
B.
CFU/mg or CFU/ml (log)
LUNG
LIVER
SPLEEN
BLOOD
Day 2
Day 5
WT
ΔFTL1678

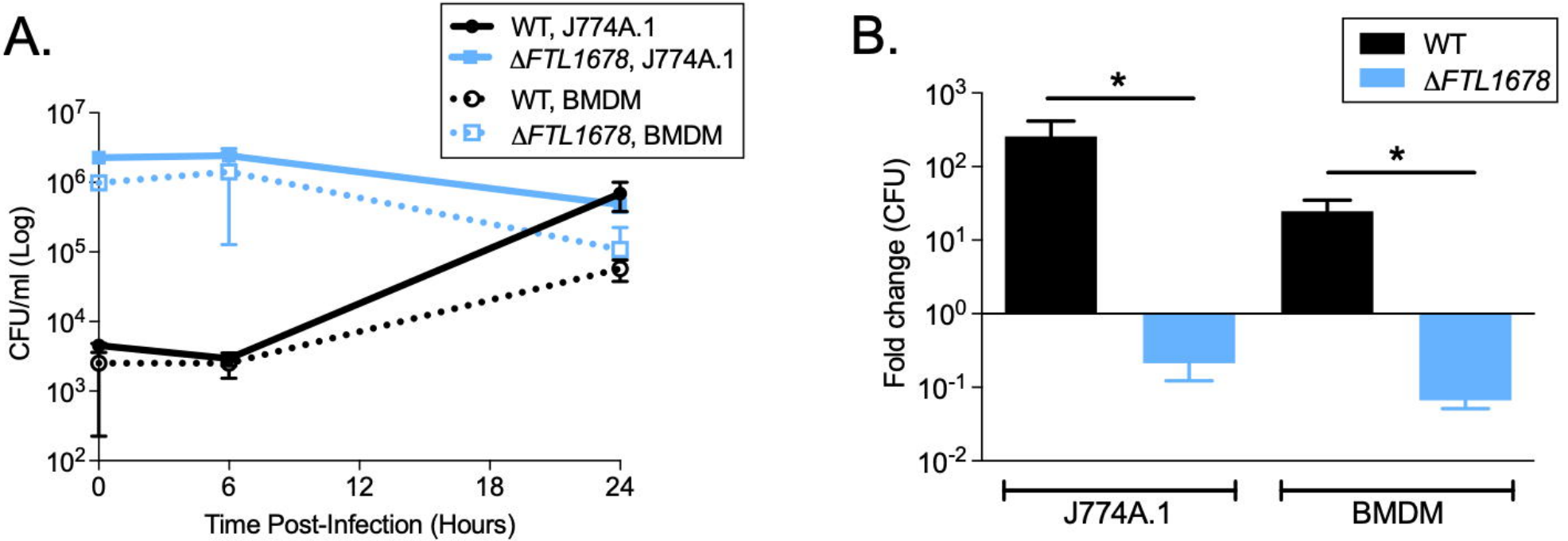
A.
WT, J774A.1
ΔFTL1678, J774A.1
WT, BMDM
ΔFTL1678, BMDM
CFU/ml (Log)
Time Post-Infection (Hours)
B.
WT
ΔFTL1678
Fold change (CFU)
J774A.1
BMDM

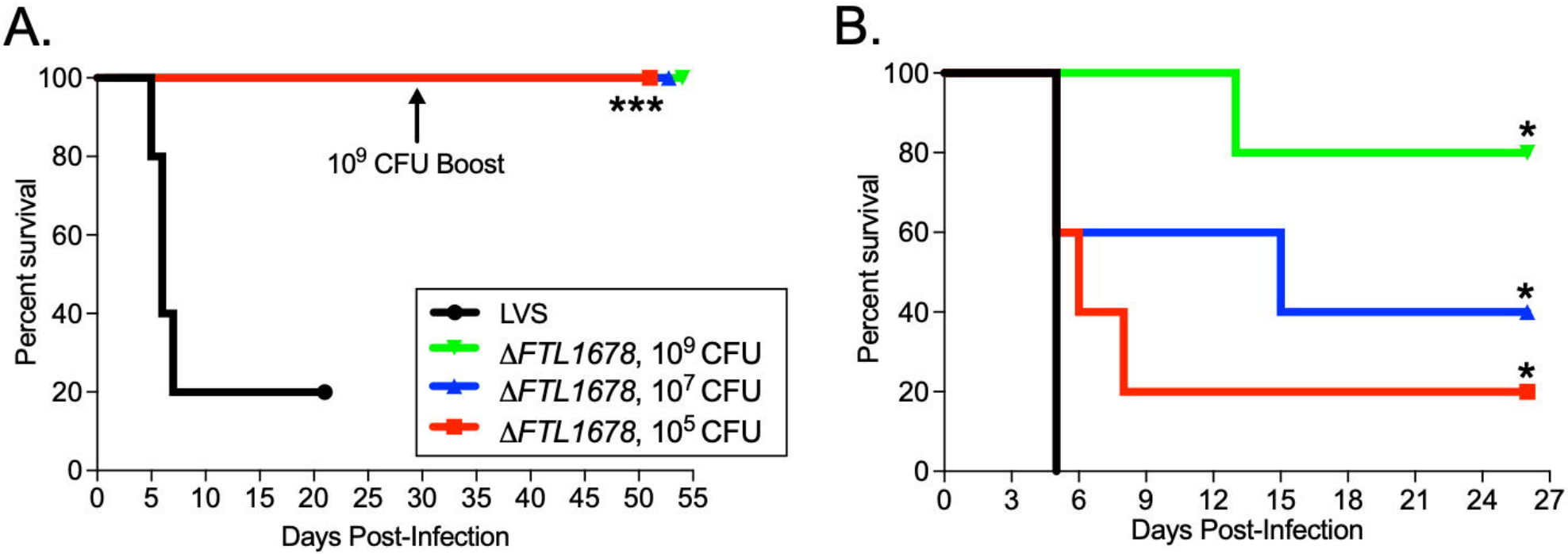
A.
100
80
60
40
20
0
Percent survival
***
10^9 CFU Boost
LVS
ΔFTL1678, 10^9 CFU
ΔFTL1678, 10^7 CFU
ΔFTL1678, 10^5 CFU
0 5 10 15 20 25 30 35 40 45 50 55
Days Post-Infection
B.
100
80
60
40
20
0
Percent survival
*
*
*
0 3 6 9 12 15 18 21 24 27
Days Post-Infection

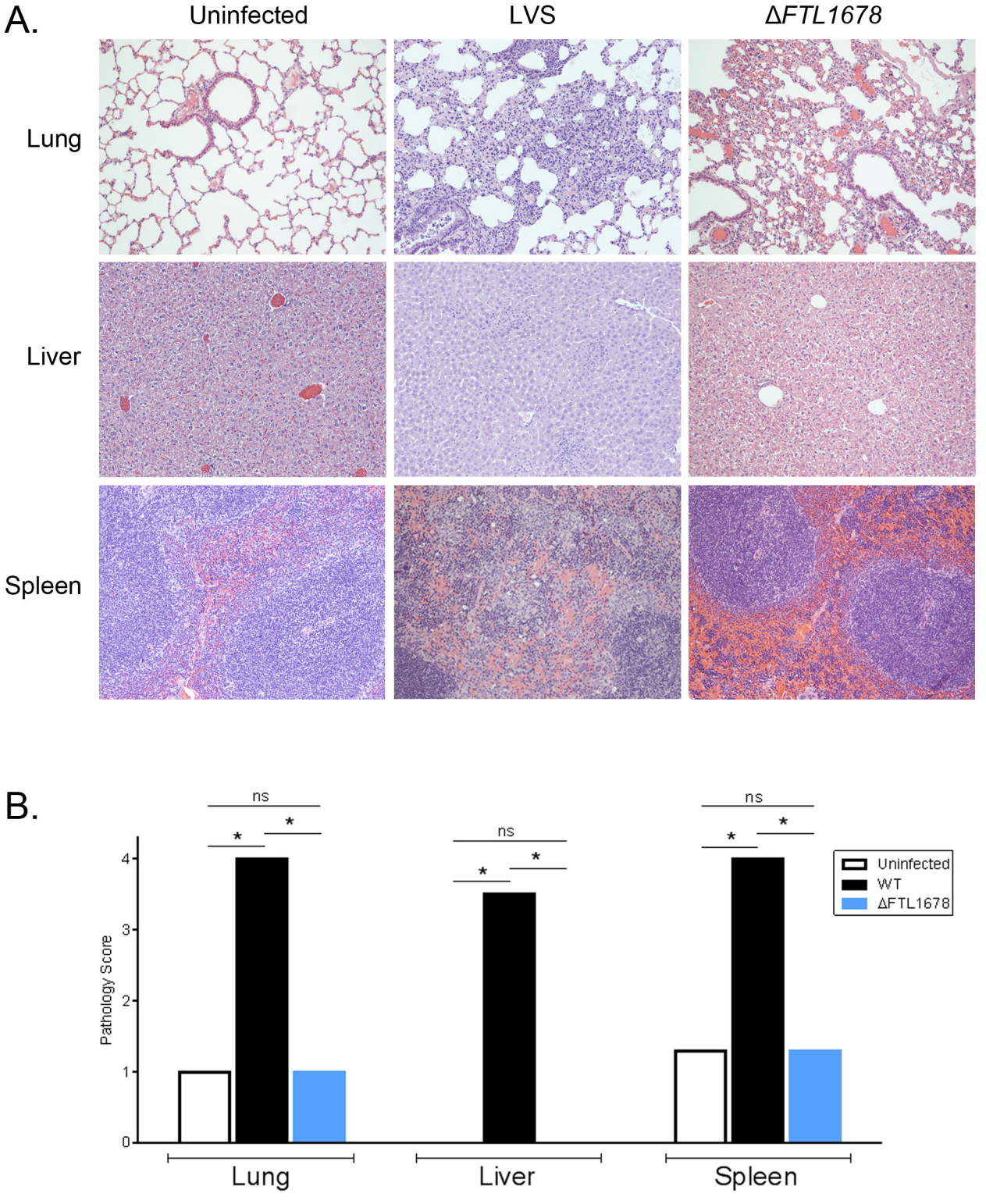
A.
Uninfected
LVS
ΔFTL1678
Lung
Liver
Spleen
B.
ns
*
*
ns
*
*
ns
*
*
Pathology Score
0
1
2
3
4
Uninfected
WT
ΔFTL1678
Lung
Liver
Spleen